Delft University of Technology
Master's Thesis in Telecommunications and Sensing Systems

Characterization of Human Blockage in 60 GHz Communication

Rizqi Hersyandika

embedded software

TU Delft Delft University of Technology

Characterization of Human Blockage in 60 GHz Communication

Master's Thesis in Telecommunications and Sensing Systems

Embedded Software Section
Faculty of Electrical Engineering, Mathematics and Computer Science
Delft University of Technology
Mekelweg 4, 2628 CD Delft, The Netherlands

Rizqi Hersyandika
rizqihersyandika@student.tudelft.nl

18th November 2016

Author
Rizqi Hersyandika (rizqihersyandika@student.tudelft.nl)
Title
Characterization of Human Blockage in 60 GHz Communication
MSc presentation
18th November 2016

Graduation Committee

prof. dr.ir. K. Langendoen (chair)	Delft University of Technology
dr. ir. R. Venkatesha Prasad	Delft University of Technology
Dr. Claudia Hauff	Delft University of Technology

Abstract

The massive availability of bandwidth in the millimeter wave (mmWave) frequency band has the potential to address the challenges posed by the unprecedented increase in the mobile data traffic. Therefore, mmWave wireless access is being seen as a promising candidate for multi-Gbps wireless access in the next generation (i.e., 5G) of wireless communications. In particular, 60 GHz frequency band with 9 GHz of unlicensed bandwidth (57–66 GHz) is being considered for the next generation of Wireless Local Area Networks (WLANs) for high data rate indoor communications. Although the 60 GHz band provides very high data rates, its signal propagation properties are quite different from the 2.4/5 GHz bands. The high free-space path loss in 60 GHz band requires directional antennas to compensate for this high path loss. Further, the small wavelengths in 60 GHz frequency band makes 60 GHz links highly susceptible to blockage due to its inability to penetrate the obstacles. For example, human shadowing overwhelmingly attenuates the received signal power and results in frequent blockages. In this thesis, we experimentally evaluate the impact of human blockage on the performance (link quality, data rate) of Commercial Off-The Shelf (COTS) 60 GHz devices.

To identify the blockages due to the human activities, we propose a reactive blockage characterization algorithm based on the observation of signal quality degradation time; and signal quality recovery time. Based on this, we categorized the blockage into: (i) short-term and (ii) long-term blockage. Our measurement results indicate that different actions are required to circumvent the link disruption caused by the long-term and the short-term human blockages. We show that in case of a long-term blockage, connecting to an alternate access point (AP) or searching for an alternate path helps in maintaining the link quality. On the other hand, in case of short-term blockage it is not advantageous to look for alternate APs or paths due to its transient nature. We also show that the incorrect detection of a blockage type aggravates the throughput performance degradation. Furthermore, we derive an important trade-off relation between the decision time and the accuracy of blockage-type detection, and show that by using an appropriate decision threshold, correct action can be executed with high detection accuracy.

Preface

What makes 60 GHz communication topic interesting is its propagation characteristic that makes the communication has to be performed in a highly directional manner. Human activities play a role in the performance of 60 GHz communication as the link blockages due to human body significantly degrade the link quality performance. The practical solution for minimizing the human blockage impact on the link quality performance is a challenging work. During this thesis project, I have learnt some theoretical knowledge about 60 GHz communication. Experimenting with a commercial 60 GHz device as well as the real human blockage make this work more interesting. I believe the results of this thesis can provide a practical approach to addressing the human blockage issue in 60 GHz communication.

First of all, I would like to thank my daily supervisor, ir. Kishor Chandra, for his guidance during this thesis project. He was always helping me to solve any technical problem and giving me the moral support. Secondly, I want to thank my supervisor, dr. RangaRao Venkatesha Prasad, for his insight and advice so that I can improve the quality of this work. My thanks also go to Prof. dr. Koen Langendoen for admitting me to this extraordinary Embedded Software group and giving me some important feedback. I also want to thank Dr. Claudia Hauff for being a committee member of my thesis. Special thanks go to my beloved wife Renya Tatiana Inaya, my daughter Athalesha Fidrizna, my parents, and family for the support they have given me. Finally, I would like to thank my friends and everybody who was involved in this work.

Rizqi Hersyandika

Delft, The Netherlands
18$^{\text{th}}$ November 2016

Contents

Chapter 1

Introduction

The rapid proliferation of mobile devices and unprecedented increase in the use of bandwidth-hungry applications have resulted in a massive growth in mobile data traffic. It is expected that by the year 2020, the total data traffic will reach 1000 times that of the year 2010. Although many advanced techniques such as Multiple Input Multiple Output (MIMO), channel bonding and frame aggregation have been proposed to enhance the data rates of the existing communication systems operating below 6 GHz (WiFi, LTE, etc.), the amount of available spectrum in the sub-6 GHz band is not sufficient to fulfill the desired growth in the network capacity.

On the other hand, a large bandwidth is available in the millimeter wave (mmWave) frequency band ranging from 30 GHz to 300 GHz, that can be utilized to enable multi-Gbps wireless connectivity. In particular, the unlicensed band in 57–66 GHz referred as 60 GHz band, provides a large bandwidth (up to 9 GHz depending on the country). Table 1.1 shows that the total bandwidth provided by the 60 GHz band is 100 and 14 times larger than those provided by the 2.4 GHz and 5 GHz bands, respectively. Therefore, it has emerged as a potential candidate for short range high data rate communications as well as multi-Gbps wireless access in the 5G era [1, 2, 3, 4].

solution for short range high data rate communications.

Band	Frequency range	Total bandwidth
2.4 GHz	2400–2490 MHz	90 MHz
5 GHz	5170–5835 MHz	665 MHz
60 GHz	57–66 GHz	9 GHz

Table 1.1: Available bandwidth provided by unlicensed WiFi bands

Due to small wavelengths, 60 GHz signal propagation is significantly different from the sub-6 GHz signal propagation. Firstly, the free-space path loss is very high at the 60 GHz band. The received signal power P_R follows

Friis transmission equation as shown below.

$$P_R = P_T G_T G_R \left(\frac{\lambda}{4\pi R} \right)^2 \tag{1.1}$$

P_T, G_T, G_R, λ and R represent the transmit power, transmitter gain, receiver gain, wavelength, and the distance between transmitter and receiver, respectively. Since P_R is proportional to λ^2 and frequency $f = c/\lambda$, then P_R is inversely proportional to f^2. Comparing P_R in a 60 GHz system with those in both conventional 2.4 and 5 GHz systems, the 60 GHz link suffers 27.96 dB and 21.58 dB higher path loss than 2.4 GHz and 5 GHz. Secondly, 60 GHz signals are very susceptible to blockage from obstacles such as humans.

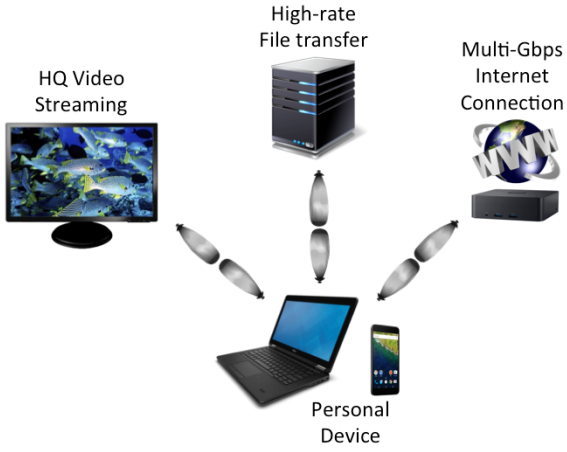

Figure 1.1: 60-GHz WPAN application

Fortunately, due to the smaller wavelengths in mmWave bands, antenna elements can be closely packed to form high-gain directional antenna arrays that can compensate for the high path loss. This compact size antenna array makes it easy to implement a 60 GHz radio chipset in our personal devices such as laptops and smartphones as well as other appliances such as TV, projector, portable data storage or wireless router. Figure 1.1 shows an example of the 60 GHz application for Wireless Personal Area Network (WPAN). Multi-Gbps data rate provided by 60 GHz communication enables wireless high definition video streaming, high-rate file transfer between devices and high-speed internet.

To leverage the available bandwidth in the 60 GHz band, several 60 GHz standardization efforts such as IEEE 802.11ad [5], IEEE 802.15.3c [6], and ECMA-387 [7] have been completed that provide Physical (PHY) and Medium Access Control (MAC) layer specifications. Among those standards, IEEE 802.11ad is the most widely used by the current 60 GHz devices because of its backward compatibility with the legacy WiFi standard (IEEE

802.11b/g/n/ac). The IEEE 802.11ad standard supports a maximum data rate of 6.756 Gbps, which is more than 10–20 times the data rate supported by the current IEEE 802.11n/ac.

1.1 Problem Description

The small wavelength and the usage of narrow beams in 60 GHz communication make it vulnerable to blockage, especially the blockage due to the human body. Several measurement studies have reported that human blockage can attenuate the signal power by 20–36 dB[8, 9, 10].

The effect of human blockage on a 60 GHz link depends on various human activities. For example, a transient blockage resulting from a human walking across the link causes a temporary link disruption. On the other hand, a permanent blockage caused by a person standing in between the link for a long duration might cause long-term link disruption. Hence, the primary objective of this thesis is to characterize and categorize the human blockage in 60 GHz links based on human activity and its effect on the link quality performance. By characterizing the blockage, a a 60 GHz device can identify the blockage type and determine an action that has to be taken to circumvent the blockage.

The permanent human blockage might cause a long-term link disruption. In IEEE 802.11ad, there are several mechanisms for addressing the long-term blockage issue such as relay and Fast Session Transfer (FST). However, most of the current 60 GHz devices that are available in the market have neither the relay nor FST mechanism ability. Therefore, in this thesis, we try to solve the long-term blockage issue by using another approach, which is handover between 60 GHz access points.

1.2 Contribution

The main contributions of this thesis are summarized as follows:

1. We provide a comprehensive review of 60 GHz experimental studies by considering various factors such as hardware used, environment, parameters measured and issues solved.

2. We conducted extensive measurements to characterize the effects of human blockage on 60 GHz links using a Commercial Off-The-Shelf (COTS) 60 GHz device based on the IEEE 802.11ad standard. To study the properties of our 60 GHz device, several experiments to measure the association time, directional coverage, and the maximum communication range are conducted. Furthermore, we also present experimental studies regarding other 60 GHz related issues such as

the effect of misalignment on directional 60 GHz links and co-channel interference.

3. We propose a human blockage characterization method to distinguish between a temporary and permanent human blockage in both Line-of-Sight (LOS) and Non-Line-of-Sight (NLOS) environments. The blockage characterization is based on the changes in the signal quality performance. It enables a 60 GHz station (STA) to determine the further action that has to be taken for minimizing the link disruption period due to the blockage.

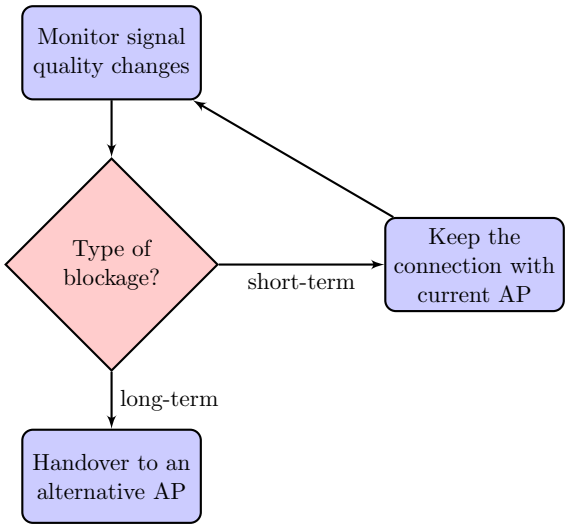

Figure 1.2: Dealing with 60 GHz link blockage

Based on the duration of link disruption, the human blockage can be categorized into two types: short-term and long-term blockage. Figure 1.2 describes how a 60 GHz station has to react following each blockage type. In the case of short-term blockage, the station waits until the signal quality recovers by maintaining the connection with the current Access Point (AP). On the other hand, in the case of long-term blockage, maintaining the connection with the current AP results in a long-period link disruption, hence an alternate AP (if available) is selected.

4. We propose a handover mechanism between 60 GHz APs to overcome the long-period link disruption due to the long-term blockage. It enables a STA to immediately look for and switch to an alternative AP in case the primary link is obstructed. We design our handover process based on the hard handover principle.

5. We evaluate our blockage characterization method in terms of the accuracy of blockage-type detection and the link downtime resulting

from each blockage type. We found a trade-off between the decision waiting time and the detection accuracy. The optimum decision time is then obtained so that the waiting time can be minimized while the high detection accuracy can be kept high.

1.3 Thesis Organization

The rest of this thesis is organized as follows. In Chapter 2, the background information about 60 GHz communication and the related work are provided. In Chapter 3, we explain about our measurement setup and show the measurement results of human blockage effect on 60 GHz link. Following that, the blockage characterization method is explained in Chapter 4. The performance of blockage characterization is evaluated in Chapter 5. Finally, we conclude with general remarks and future work in Chapter 6.

Chapter 2

Background and Related Work

In this chapter, we provide background information and research work related to 60 GHz communication. Firstly, the propagation characteristic in 60 GHz band is described. In this band, the signal suffers higher path loss compared to that in the lower band so that the communication in the 60 GHz band needs to be highly directional. Secondly, a standardization effort in 60 GHz communication, IEEE 802.11ad, is explained. This standard provides the information about channelization in 60 GHz band, PHY and MAC layer specifications, and a mechanism called beamforming training that is used to establish a directional communication. Following that, the link blockage issue in 60 GHz and how the current 60 GHz standard can deal with the blockage are discussed. Finally, a comprehensive review of the 60 GHz experimental studies by considering various factors such as hardware used, environment, parameters measured and issues solved is provided.

2.1 Propagation Characteristic of 60 GHz

Millimeter Wave (mmWave) band ranges from 30–300 GHz. In this band, the propagation suffers higher attenuation due to atmospheric gases, including oxygen and water/rain absorptions, when compared to the lower frequency band. For the frequency below 100 GHz, total atmospheric gases attenuation reaches its peak (around 15 dB/km) at 60 GHz[11] as indicated by the green rectangle in Figure 2.1. Therefore, this attenuation characteristic theoretically limits the usage of 60 GHz frequency band for long-range communication.

Small wavelengths in 60 GHz band results in the two following propagation issues: high free-space path loss and high penetration loss. The latter makes the signal difficult to penetrate into an obstacle, including the human body, as discussed further in Section 2.3. As shown in Equation 1.1, the re-

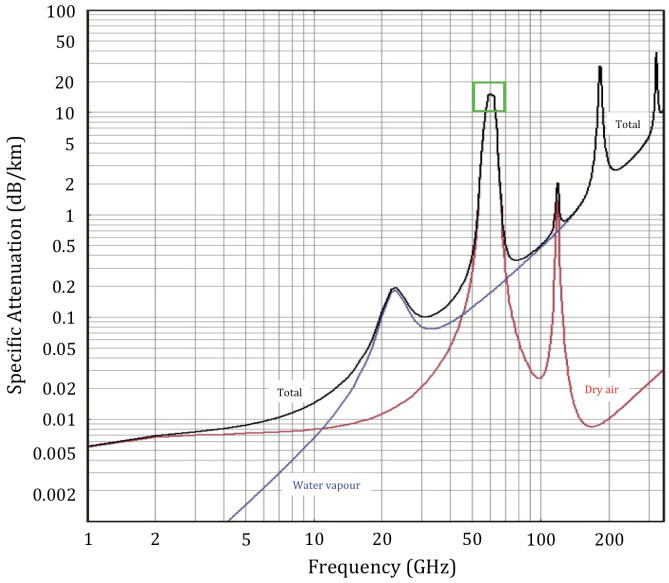

Figure 2.1: Atmospheric attenuation in 60 GHz [11]

ceived signal power P_R is inversely proportional to f^2. The comparisons of received signal power in 60 GHz with those in 2.4 GHz and 5 GHz are shown in Equation 2.1 and 2.2, respectively.

$$\frac{P_{R(f=60\ GHz)}}{P_{R(f=2.4\ GHz)}} = \left(\frac{2.4\ GHz}{60\ GHz}\right)^2 = 0.0016 = -27.96\ dB \tag{2.1}$$

$$\frac{P_{R(f=60\ GHz)}}{P_{R(f=5\ GHz)}} = \left(\frac{5\ GHz}{60\ GHz}\right)^2 = 0.00694 = -21.58\ dB \tag{2.2}$$

The equations above show that the radio signal in 60 GHz band suffers 27.96 dB and 21.58 dB additional path loss compared to those in 2.4 GHz and 5 GHz bands, respectively.

To compensate for the high path loss, a highly directional antenna has to be used at each transmitter (Tx) and receiver (Rx) [12]. The directivity gain depends on the number of antenna elements. The more antenna elements used, the narrower beam that can be formed to focus the energy in a particular direction. Hence, higher directivity gain can be achieved. Furthermore, the use of narrow beam minimizes the interference between 60 GHz links and thus provides high spatial reuse. However, according to FCC regulation [13], the maximum allowable EIRP for a 60 GHz device is limited to 40 dBm.

The usage of narrow beam in 60 GHz link requires the transmission path to be LOS since the beam of Tx and Rx has to be pointing each other to get the maximum directivity gain. However, a 60 GHz link does not only rely on the LOS transmission path but also able to utilize NLOS transmission

path from the reflected signal. The first-order and second-order reflected signal reduce the received signal power by approximately 10 dB and 20 dB, respectively [14]. Therefore, the reflected signal, especially the first-order reflection, is potential to become an alternative transmission path in case the LOS path is unavailable.

2.2 IEEE 802.11ad Standard

To leverage the available bandwidth in 60 GHz band, several 60 GHz standardization efforts such as IEEE 802.11ad, IEEE 802.15.3c, and ECMA-387 have been completed. IEEE 802.11ad [5] and IEEE 802.15.3c [6] are the task groups under IEEE formulating the standardization of PHY/MAC for 60 GHz Wireless Local Access Networks (WLANs) and Wireless Personal Access Networks (WPANs), respectively. However, IEEE 802.15.3c task group was hibernated in November 2009 [15]. Meanwhile, ECMA-387 [7] provides PHY, MAC and HDMI Protocol Adaptation Layer (PAL) standard for 60 GHz wireless networks. The comparison of PHY, MAC and network architecture between those three standards are discussed by K. Chandra et al. [16], in which IEEE 802.11ad is more favored to lead the 60 GHz communication because of its backward compatibility with the previous WiFi standard (IEEE 802.11 b/g/n/ac).

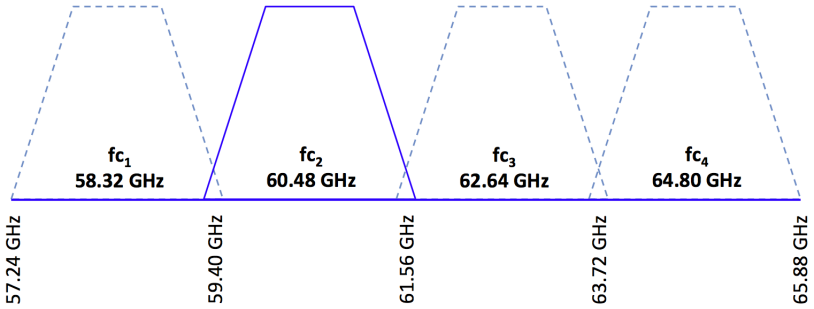

Figure 2.2: Channelization in 60 GHz band

IEEE 802.11ad operates in 57–66 GHz consisting of 4 available channels (depending on the country) with the channel bandwidth of 2.16 GHz. Channelization in 60 GHz band is shown in Figure 2.2. This standard supports the data rate up to 6.756 Gbps. The achievable data rate is determined by 32 levels of Modulation and Coding Scheme (MCS) that depends on the received signal level.

IEEE 802.11ad defines three following PHY types: Control PHY, Single Carrier (SC) PHY and Orthogonal Frequency Division Multiplexing (OFDM) PHY [5, 17, 18]. Control PHY is used to exchange the control frame during the beacon transmission and beamforming training phase, prior to the data transmission. It is defined as MCS 0 providing the maximum data rate

of 27.5 Mbps. SC PHY is used for the data transmission and is designed for low-complexity and low-power transceivers. MCS 1–12 and MCS 25–31 represent the SC PHY and low-power SC PHY, respectively, providing the data rate from 385 Mbps to 4.62 Gbps. Meanwhile, OFDM PHY is used for higher data rate performance. It is represented by MCS 13–24 providing the data rate from 693 Mbps to 6.756 Gbps. The modulation type, code rate, achievable data rate and the required receiver sensitivity for all MCS indexes are shown in Appendix A.

2.2.1 Beamforming Training

As explained previously in Section 2.1, to compensate for the high path loss in 60 GHz frequency band, the transmission has to be highly directional. The beam of Tx and Rx have to be aligned precisely to achieve high directional gain. In IEEE 802.11ad, the mechanism used for aligning the communicating station's beam is called beamforming training. Through this mechanism, a 60 GHz station (STA) determines its best beam to be used for the data transmission with its pairing STA, and vice versa. Beamforming training consists of two phases: Sector Level Sweep (SLS) and an optional Beam Refinement Protocol (BRP).

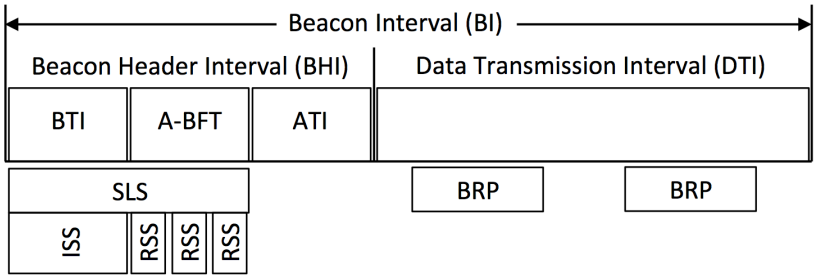

Figure 2.3: Beamforming phase during a Beacon Interval

Sector Level Sweep (SLS)

SLS is the initial phase in beamforming training with the purpose of finding the best transmitting and receiving sector of two communicating STAs. The communicating STAs exchange the Sector Sweep (SSW) frames over different antenna sectors. SLS phase occurs within Beacon Header Interval (BHI) in a Beacon Interval (BI) as described in Figure 2.3. During SLS phase, Control PHY is used.

SLS consists of two main steps: Initiator Sector Sweep (ISS) and Responder Sector Sweep (RSS). An initiator is a STA that initiates the beamforming training by transmitting SSW frames while a responder is a STA that receives the SSW frames transmitted by the initiator. Both initiator and

responder can be either performing Transmit Sector Sweep (TXSS) or Receive Sector Sweep (RXSS). In the case of asymmetrical link, in which the best transmitting sector of a STA might be different from its best receiving sector, both TXSS and RXSS have to be conducted.

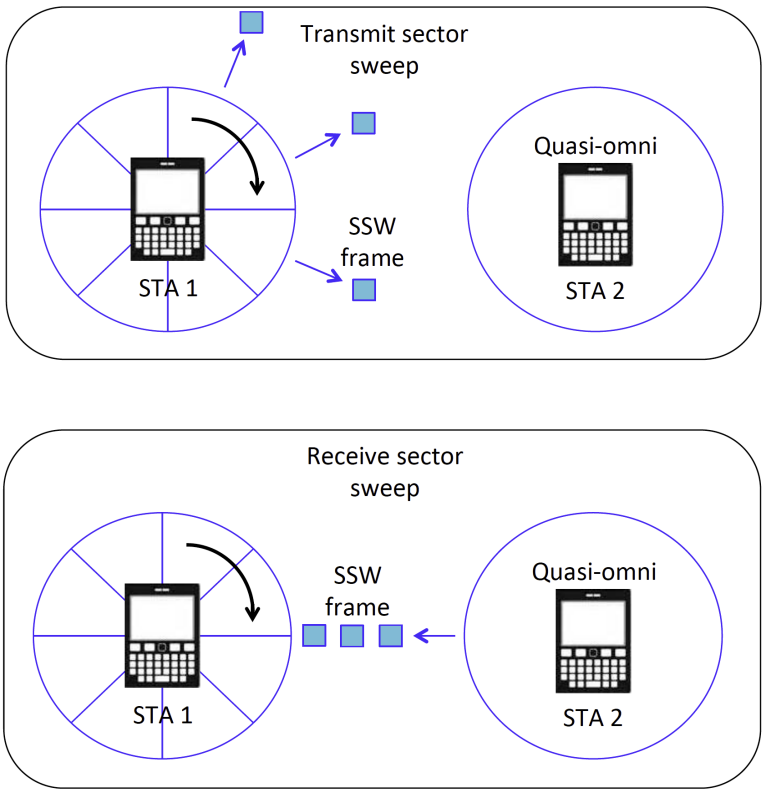

Figure 2.4: TXSS and RXSS procedure in SLS phase

TXSS and RXSS procedures are depicted in Figure 2.4. In TXSS, a transmitting STA (STA_1) sweeps its antenna sectors while transmitting SSW frames using its different transmitting sectors. A receiving STA (STA_2) receives the SSW frames by using its quasi-omni antenna mode. Every SSW frame transmitted by STA_1 is marked with its sector ID and antenna ID so that STA_2 can identify the best transmitting sector of STA_1. In RXSS, STA_2 transmits SSW frames using its quasi-omni antenna mode, while STA_1 sweeps its antenna sector for receiving such SSW frames. These SSW frames contain information about STA_1's best transmitting sector that is indicated previously by STA_2. After finishing RXSS, STA_1 sends an acknowledgement containing the information about STA_1's best receiving sector to STA_2. Therefore, in the end, both STAs know about STA_1's best transmitting and receiving sector. The similar procedure has to be performed in the STA_2's side to obtain STA_2's best transmitting and receiving sector. The more numbers of sectors a STA intends to train, the more SSW frames required.

Beam Refinement Protocol (BRP)

BRP is an optional phase in beamforming training that aims to improve the Tx and Rx antenna configuration by iteratively refining Antenna Weight Vectors (AWV) of the transmitting and receiving sectors at both communicating STAs. It can also be used to train the receiving STA's antenna sector in case it has not been done in the previous SLS phase. BRP phase takes place within Data Transmission Interval (DTI) as described in Figure 2.3.

BRP consists of these following subphases: BRP setup, Multiple sector ID Detection (MID), Beam Combining (BC) and beam refinement transaction. BRP setup is used to request the execution of MID or BC subphase. In MID subphase, a transmitting STA uses quasi-omni mode while the receiving STA sweeps its Rx AWV configuration. This procedure is similar with RXSS in SLS phase. In BC subphase, both transmitting and receiving STAs test their multiple Tx AWVs and Rx AWVs to find the best combination of Tx AWV and Rx AWV among them. Lastly, beam refinement transaction subphase is used to exchange the beam refinement request and response.

2.3 Link Blockage in 60 GHz

Link disruption in 60 GHz communication is caused by two factors: beam misalignment and link blockage. Beam misalignment can be caused by the user movement such as rotation or displacement. Meanwhile, in link blockage, the beam is blocked by an obstacle leading to the degradation of link quality. Both factors make the beam pair between two communicating STAs becomes no longer supporting the communication.

Several studies have been performed in distinguishing the causes of link outage in 60 GHz communication. Tsang et al. [19] distinguish between the link outage due to the device mobility and the human blockage without any external aid from GPS or sensor. They make use the rate of signal power drop and the validity of beam selection. Meanwhile, Doff et al. [20] employ the motion sensor to determine the cause of beam errors and predict the beam selection for the next transmission based on the user's motion.

As mentioned in Section 2.1, the small wavelength in 60 GHz band results in high penetration loss that makes the signal difficult to penetrate into an obstacle such as the wall, furniture and the human body. The human body potentially causes a shadowing effect in 60 GHz LOS transmission path. It causes an additional 20–36 dB attenuation [8, 9, 10] and thus significantly reduces the received signal power. The obstruction duration caused by human body blockage ranges from 370–820 ms [10]. Several studies in modelling the human body blockage in a 60 GHz link are performed [21, 22, 23, 24]. For example, Gustafson et al. [23] uses a phantom filled with water to model the human body blockage as it has similar shadowing and reflection properties

to the real human body.

To respond the link blockage, a STA can perform either proactive or reactive action. In the proactive method, the STA continuously monitors the link, predicts when the blockage will occur and takes an action before the link quality decreases due to the blockage. Usually, this method requires an external aid such as sensor or camera. Oguma et al. [25] uses RGB-D cameras for predicting the position, velocity, and direction of moving pedestrians so that the STA can switch to another AP before the pedestrians block the LOS path. On the other hand, in the reactive method, the action is only taken immediately after the link quality degradation due to the blockage is detected. In this case, the signal has already been attenuated due to the obstruction. However, no additional aid is required in this method.

IEEE 802.11ad has the three following mechanisms in dealing with link blockage:

1. **Beam switching**: When there is a link blockage in the LOS transmission path, the signal quality decreases below a certain threshold. It triggers the communicating STAs to perform beamforming training to search for an alternative beam pair. The alternate beam pair can be obtained through a NLOS transmission path (e.g. reflection from the wall). However, in case the obstacle area is large enough to completely obstruct the beam or in case no alternative path exist, then the beam switching mechanism can not overcome such blockage problems.

2. **Relay**: An additional STA can be used for relaying the transmission in case the LOS transmission path (direct link) is blocked. The transmission from a source STA towards a destination STA is forwarded by a relay STA. There are two types of relay operations specified in this standard: link switching and link cooperating. In the link switching method, the transmission is switched from a direct link to the relay link after the direct link suffers an outage. Meanwhile, in the link cooperating method, the relay links are actively involved in the direct transmission.

3. **Fast Session Transfer (FST)**: FST enables a STA to switch to the 2.4 or 5 GHz band when it suffers link outage. It is because IEEE 802.11ad is backward compatible with the legacy WiFi standard and supports multi-band operation. However, in this mechanism, the link will experience a significant degradation of data rate, from multi-Gbps to a hundred of Mbps.

S. Sur et al. [26] propose BeamSpy, an algorithm to predict the quality of alternative beams by observing the channel impulse response of each beam. It reduces beam searching overhead during the beam switching procedure. BeamSpy algorithm is implemented in a programmable 60 GHz radio platform called WiMi. Congiu et al. [27] analyze the benefit and drawback of

using a relay and FST mechanism. Relay option is preferred for a network with high traffic and low beam training overhead while the FST option is more suitable for a network with low traffic and low blockage probability.

2.4 60 GHz Experimental Related Work

We provide a comprehensive review of 60 GHz experimental studies concerning the hardware used, environment, parameters measured and issues solved. We categorize the hardware used into two types: COTS and customized hardware. The COTS hardwares commonly used for the experiment are wireless docking stations with the 60 GHz radio chipset manufactured by Wilocty. Meanwhile, for the customized hardware, the setup mainly consists of a signal generator, 60 GHz transceiver, and the directional antenna. The additional receiver or signal analyzer might be used to observe some parameters. The parameters measured are the received signal quality, PHY link rate, application layer throughput, frame level as well as the latency.

Most of the experiments are conducted in indoor environments such as home, office and the data center. Meanwhile, only a few of them discuss about the feasibility of 60 GHz application in the outdoor environment. Several issues discussed are the communication range, deafness effect, interference, human blockage, user movement and the beamforming overhead. The detailed review of 60 GHz experimental studies is shown in Appendix B.

Saha et al. [29] analyze signal quality and throughput performance against the distance and height diversity in the indoor environment using COTS 60 GHz device. Besides that, the effect of human blockage and channel interference are also investigated. Nitsche et al. [30] observe frame level, beam pattern, reflections, and interference. They use two different COTS 60 GHz systems: (i) Wireless Docking System (WiGig) and (ii) WirelessHD. An additional receiver is used to measure the received signal power over the air and to analyze the frame. The frame loss and retransmission monitored indicates the interference between two systems. The inter-system interference occurs because WiHD system does not use CSMA/CA and thus blindly transmits data causing collision to WiGig system. Ansari et al. [31] perform an experimental study of the throughput and BER performance for the indoor 60 GHz network. They experimented with the three different customized 60 GHz transceivers: Hittite Microwave HMC6000/1 with on-chip antenna providing 38 dB gain, SiversIMA FC1005V/00 and HXI GigaLink 6651. The last two setups are equipped with two types of horn antenna providing 10 dBi and 25 dBi gain. The results show that BER increases when higher sub-carrier modulation is used. It is because high sub-carrier modulation requires a high Signal-to-Noise Ratio (SNR). Loch et al. [32] study the effect of deafness due to the directionality in mm-wave networks. The author uses two

pairs of Wireless Docking System to recreate the deafness scenario between two 60 GHz links. Ostinato program is used for generating data streams and Wireshark is utilized for the delay jitter measurement. The results show that as the level of frame aggregation increases, the throughput fairness between two 60 GHz links can be achieved. It is because the less number of packets makes the collision occurs less frequently despite the deafness.

Maltsev et al. [14] perform an experimental investigation of 60 GHz WLANs in the office environment (conference room and cubicle) without the presence of human activity. The results show that the first-order and second-order reflected signal reduce the received signal power by approximately 10 dB and 20 dB, respectively and thus can still provide sufficient SNR for the communication. Halperin et al. [33] propose wireless flyways mechanism by adding extra capacity using the 60 GHz wireless network to alleviate the oversubscribed link in the data center. To that end, they use customized 60 GHz HXI radios that are placed on top of the server racks. They investigate the throughput stability, interference and security of the 60 GHz network usage inside the data center. The separation distance between two parallel links using the same frequency should be sufficient to avoid co-channel interference. In addition, the usage of different channels in each link and highly directive antenna can reduce the separation distance. Still related to the 60 GHz application in the data center, Zhu et al. [34] propose Angora, which is a static 60 GHz wireless link connecting server racks for providing control traffic in the data center. The results confirm that the angular separation plays an important role for minimizing the interference between two 60 GHz links, in which larger angular separation results in lower throughput loss.

For the outdoor environment, Y. Zhu et al. [35] investigate the feasibility of 60 GHz picocell implementation in an urban environment. The measurements are performed using both COTS and customized 60 GHz devices. Range, user motion, blockage, and interference are observed. In this work, the authors dispel common myths about the feasibility of 60-GHz picocell such as the range limitation in the outdoor environment and the difficulty in achieving robust communication due to user mobility and link blockage. Simic et al. [36] investigate the beam steering requirement in the mm-wave urban outdoor environment (residential and commercial urban area) that consists of a heterogeneous mix of building materials. The various locations are chosen in order to observe both LOS and NLOS transmission paths. The results show that 10° misalignment degrades the achievable data rate by 20–100 %. Therefore, the beam steering between Tx and Rx is required to overcome this beam misalignment issue.

In this thesis, we investigate the effect of human blockage in 60 GHz link and propose a method for characterizing the blockage based on the observation of the signal quality degradation and the signal quality recovery. The blockage characterization aims to reduce the link disruption effect due to each blockage type. To that end, we perform experimental measure-

ments using COTS 60 GHz wireless docking station equipped with Intel-manufactured 60 GHz radio chipset. The experiments are conducted in indoor environments with LOS and NLOS scenarios. The normalized signal quality and link throughput performance are measured.

Chapter 3

Link Blockage Effect Measurements

In this chapter, we provide measurement results using the Dell devices (laptops and docking station) that are equipped with the 60 GHz IEEE 802.11ad chipsets. Our measurement results consists of: (i) preliminary measurements to characterize the communication range, directional coverage patterns, connection establishment time, effect of misalignment on the link quality and beam re-alignment time of the devices used; (ii) effects of co-channel interference on the link performance when two links are operating in a close proximity; and (iii) effect of human shadowing on the link performance considering temporary and permanent human blockages. For the preliminary and the co-channel interference measurements, we only consider LOS scenarios while the human blockage measurement were conducted when both the LOS and NLOS paths were available. We used the received signal quality and link throughput as the parameters to discuss the measurement results.

3.1 Measurement Methodology

The measurements were conducted in a hall with the dimension of 9 x 5 x 4 m, where no reflection and only LOS transmission path between two communicating devices were expected. However, since we can not control the beam direction and the beam switching process, there is a possibility that the devices will establish a NLOS transmission path as a result of the signal reflected-off the wall. We performed the measurement with the separation distance between the two devices (d) of 3 and 7 m to observe the effect of the distance variation on the link quality degradation. The human blockage was introduced in the middle of the distance between the two devices (d) at a height of 1.2 m. To observe the link quality degradation, we measured two following parameters: (1) Normalized signal quality and (2) Throughput.

3.1.1 Hardware

To create a 60 GHz network, we use a COTS 60 GHz wireless docking system consisting of a pair of Dell WLD15 wireless docking station and Dell Latitude E7450 laptop as shown in Figure 3.1. The docking station and the laptop act as the Access Point (AP) and the wireless station (STA), respectively. These devices can establish a point-to-point wireless connection in which one laptop can only connect to one docking station at a time, and vice versa. The wireless docking stations are designed to reduce the wire usage and increase the user mobility when connecting the laptop to multiple devices such as the monitor, portable data storage, and router. This wireless docking station enables the wired connection to display monitor (via HDMI, miniDP or VGA port), portable data storage (via USB 2.0 or USB 3.0 port) and Ethernet router/switch (via Gigabit Ethernet port).

Figure 3.1: COTS 60 GHz wireless docking system

The docking station and laptop are equipped with Intel Wireless Gigabit Sink W13100 dock module [37] and Intel Tri-Band Wireless-AC 17265 radio chipset [38], respectively. It supports three channels in the 60 GHz band with the following center frequencies (f_c): 58.32 GHz, 60.48 GHz, and 62.64 GHz. For the experiment, we use the third channel. Its beamforming and rate adaptation mechanism are based on the IEEE 802.11ad standard. It uses Control PHY (MCS 0) to exchange the control frame and Single Carrier PHY (MCS 1-12) for the data transmission supporting the data rate of 385–4620 Mbps, as indicated in Table A.1. By default, this system automatically perform beam switching to find an alternative beam (transmission path) if it detects the signal quality degradation.

Limitations

This wireless docking system does not enable the user to access the lower layer (PHY and MAC) information. It comes with an Application Programming Interface (API) providing very limited information about the link quality parameters. Unlike the other wireless docking system whose radio

chipset is manufactured by Wilocty [29, 30, 35], the Intel-manufactured wireless docking system does not provide PHY data rate information. Instead, the only information about the link quality is represented by the normalized signal quality parameter in the scale of 0 to 10. Moreover, the Gigabit Ethernet port available in the AP limits the data rate to 1 Gbps. Therefore, it becomes a bottleneck when measuring the actual link rate since a multi-Gbps data rate provided by the 60 GHz connection can not be achieved. Moreover, our 60 GHz wireless docking system does not support the relay and FST mechanism.

3.1.2 Signal Quality Measurement

Information about the link quality is provided by Intel Wireless Gigabit (WiGig) driver (version of 2.0.30.62). To extract the signal quality information, we make use *WiGigSDKWPFWrapper.dll* file that provides access to the WiGig driver. Figure 3.2 depicts the procedure for obtaining the signal quality information. During the measurement, the signal quality was recorded per 1 ms interval so that the changes of signal quality that occurring within millisecond order can be captured.

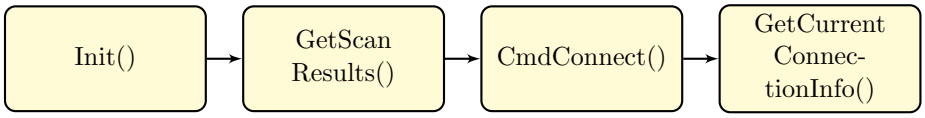

Figure 3.2: Signal quality measurement procedure

The first step in getting the connection information is to initialize the communication with the driver, that is executed by *Init()* class. The next step is to establish the connection with an AP. By default, a STA automatically scans all available APs within its range and creates a list called *ScanPeerSdk[]* containing MAC addresses of all available APs. We use *GetScanResults()* class for querying the scan results listed in *ScanPeerSdk[]*. Upon detecting at least one AP on its scanning list, the STA immediately attempts to connect to that AP by using *CmdConnect()* class. In this phase, both STA and AP perform beamforming training procedure to find the best beam pair between them.

After the connection establishment process finished, the signal quality information is obtained by using *GetCurrentConnectionInfo()* class. The output type of the signal quality parameter is Int32. Besides the normalized signal quality information, *GetCurrentConnectionInfo()* also provides the performance quality indicator in terms of *"Good"*, *"Improvable"* and *"Insufficient"*, as well as the current active channel that is being used.

3.1.3 Throughput Measurement

Throughput refers to the amount of data (in bits or Bytes) delivered through the network for a given amount of time. To measure the throughput, we use TCP traffic that is generated and measured by Iperf3 (version 3.1.3) [39]. Figure 3.3 depicts the throughput measurement setup between STA and AP. An additional laptop (Macbook Air OS X 10.9.4) generating and sending the TCP traffic is connected to the docking station via Gigabit Ethernet interface. The docking station uses Realtek USB GBE Family Controller driver version 7.6.1009.2013.

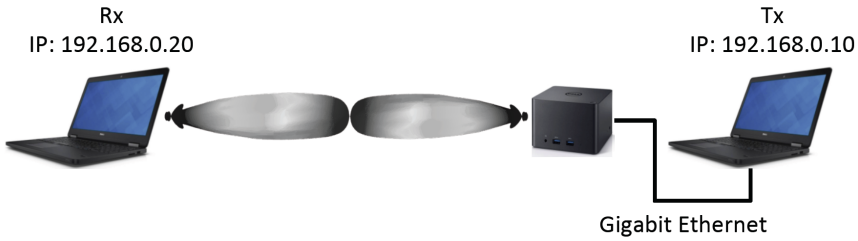

Figure 3.3: Throughput measurement setup

A static IP address is assigned in each laptop for enabling the IP communication between the server and client. In our configuration, the laptop connected to the docking station through the 60-GHz link (IP address: 192.168.0.20) becomes the Iperf3 client while the additional laptop attached to the docking station via Gigabit Ethernet interface (IP address: 192.168.0.10) becomes the Iperf3 server. Most of the configuration parameters are set in the Iperf3 client side. The following example command is used for running Iperf3 on the client side:

```
iperf3 -c 192.168.0.10 -b 1000m -w 3728270 -t 30 -i 0.1 -R
```

192.168.0.10 refers to the server's IP address. *"-b 1000m -w 3728270"* indicate the maximum bandwidth of 1 Gbps and the TCP window size of 3728270 Bytes, respectively. The measurement duration is 30 s with the reporting interval of 100 ms as indicated by *"-t 30 -i 0.1"* command. Normally, the client becomes the traffic sender, and the server becomes the receiver. However, we use the reverse mode, indicated by *"-R"* command, so that the server sends the traffic to the client. Therefore, in this case, the docking station becomes a Tx while the laptop becomes an Rx.

Bandwidth	1 Gbps
Maximum Segment Size	1460 Bytes (default)
TCP Window Size	3728270 Bytes

Table 3.1: TCP throughput measurement parameter

The parameters used in the TCP throughput measurement are shown in Table 3.1. Maximum Segment Size (MSS) indicates the maximum payload in a single TCP segment, excluding the IP header (20 Bytes) and TCP header (20 Bytes). For this measurement, we use the default MSS of 1460 Bytes. Meanwhile, TCP window size indicates the maximum data that can be sent by the sender before the receiver acknowledges it. In other words, it indicates the maximum buffer size at the receiver. Setting this parameter too small reduces the maximum achievable throughput. Therefore, we set the TCP window size as large as possible in which 3728270 Bytes is the maximum TCP window size supported by the system.

3.2 Preliminary Measurements

3.2.1 Association Time

Association time is the time required by a STA and an AP to establish a 60 GHz connection. It also refers to the duration of when the STA initiates the *CmdConnect()* command until the best beam pair between STA and AP is obtained. Initially, when the STA is not connected yet to the AP, the measured signal quality equals to 0. After running the *CmdConnect()* command, the association process begins. It involves the beamforming training process as explained in Section 2.2.1. During the association process, the signal quality equals to 1. After the best beam pair between the STA and AP has been aligned, the connection is established, indicated by the rising of signal quality from 1 to a certain higher value.

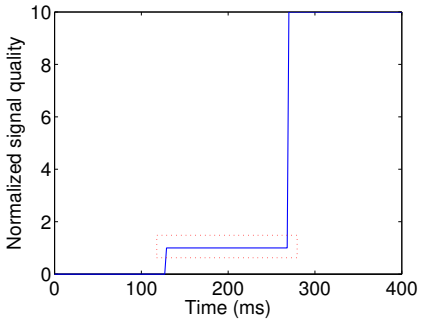

Figure 3.4: Association time

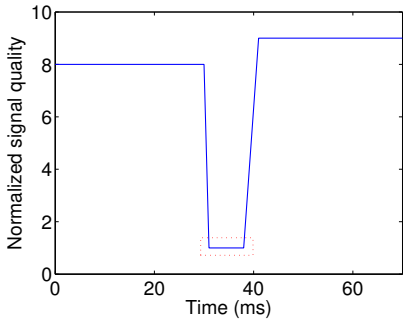

Figure 3.5: Beam re-alignment time

An example of signal quality snapshot during the association process is depicted in Figure 3.4. In this measurement, the position of STA is LOS with AP, and the distance between them is 3 m. The measurement results show that the average association time is **146.8 ms**.

3.2.2 Beam Re-alignment Time

Beam re-alignment time is defined as the time required by a STA and an AP to re-align their beam in case the beam misalignment occurs. The beam misalignment occurs if either STA or AP is rotated. As soon as STA and AP detect the link quality degradation due to the beam misalignment, they try to re-align their beam by performing the beamforming training.

To measure the beam re-alignment duration due to the rotation, the docking station was rotated by 60°, while the laptop position is kept fixed. The changes of signal quality and the timestamp in ms were recorded. The beam re-alignment time is indicated since the signal quality starts dropping to 1 as a result of beam misalignment until it reaches a certain higher value again following the beamforming training process. Figure 3.5 describes an example of signal quality snapshot during the re-alignment time. The average beam re-alignment time is **7.65 ms**.

3.2.3 Directional Coverage

During our initial investigation, we found that the 60 GHz antenna array of the laptop is located on the top left laptop's lid since it is the most sensitive area affected by the blockage. Meanwhile, for the docking station, the front side of the dock becomes the area transmitting the strongest signal power.

To measure the directional coverage of the docking station, we rotate the docking station by 360° while keeping the laptop position fixed. The signal quality is recorded for every 10° rotation angle interval. The same thing also applied for the laptop's directional coverage measurement. The measurement was conducted in an LOS environment with the distance between the docking station and laptop of 4 m. There is no traffic presence during this measurement.

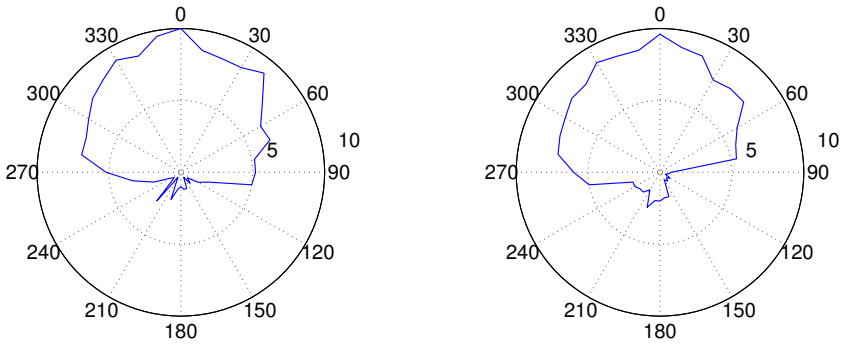

(a) Docking station (b) Laptop

Figure 3.6: Directional coverage measurement results

Figure 3.6 (a) and (b) show the directional coverage results of the docking

station and the laptop, respectively. The results show that both antenna arrays of the docking station and laptop only support 180° coverage, especially in the front area of the devices. It is indicated by the high signal quality monitored within -90° to 90° angle. In Figure 3.6(b), the laptop's directional coverage seems bit asymmetric because the antenna array of the laptop is located on the top left of laptop's lid.

3.2.4 Maximum Range

The maximum range measurement was performed by moving the STA away from the AP. As the distance between STA and AP increases, the signal quality decreases. In a certain distance, STA will be disconnected from AP due to the lack of received signal strength. That distance is referred to as the maximum range of the connection. The measurements were conducted in an empty parking lot and inside EWI building corridor to represent the outdoor and indoor environment, respectively. Two measurement scenarios: with and without the traffic presence, were performed.

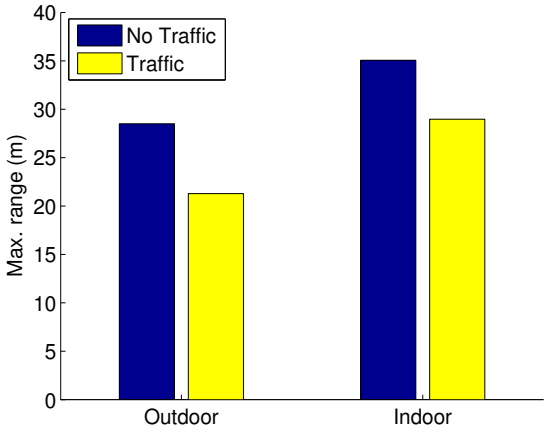

Figure 3.7: Maximum range of WiGig system

In Figure 3.7, it is shown that the average of maximum range in the indoor environment is higher than that in the outdoor environment. It is because the reflection from the wall or other objects in the corridor (indoor environment) focuses the beam pair between STA and AP and thus makes the beam more directive. Meanwhile, in the outdoor environment, the signal energy tends to spread all over the area. Therefore, the maximum communication range is longer in the indoor environment.

It is also shown that in each environment, the maximum range is always longer in the case of no traffic presence. It is because in the absence of traffic, the communication uses a low MCS allowing the lower received signal level (receiver sensitivity). On the other hand, when there is a traffic presence,

higher MCS is used. The higher MCS requires higher receiver sensitivity that makes the connection easier to be disrupted whenever the received signal level requirement can not be achieved. Consequently, with the same received signal value at a certain distance, the presence of traffic in the network shorten the maximum range.

3.2.5 Co-channel Interference

By this measurement, we would like to observe the effect of co-channel interference on the throughput performance. For this measurement, two pairs of docking stations and laptops are required. The first pair is a primary link while the other pair is an interfering link. Both 60-GHz connections are transmitting on the same channel. The traffic in the primary connection was generated by using Iperf3 while the traffic in the interfering connection was produced by the wireless file transfer from a USB stick attached to the AP.

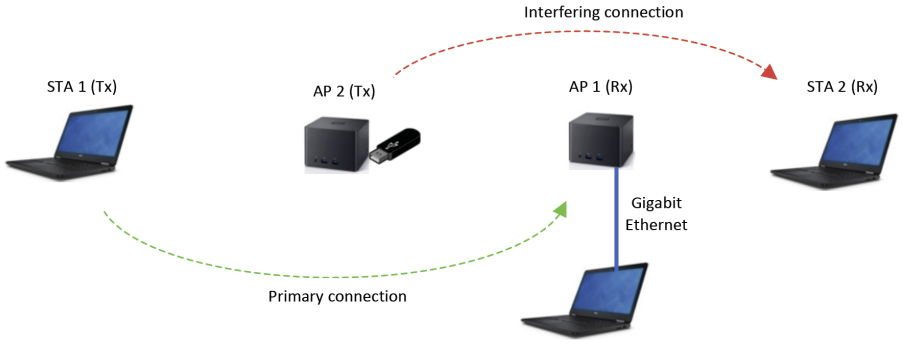

Figure 3.8: Co-channel interference scenario 1

Two measurement scenarios were performed, as depicted in Figure 3.8 and 3.9. We performed the worst case scenario where the primary link and the interfering link was positioned in a straight line with the distance between each node of 1 m. Tx of the interfering link (AP_2) is placed in the middle of Tx and Rx of the primary link (STA_1 and AP_1). In scenario 1, AP_2's transmission is directed to AP_1 which becomes an Rx in the primary link. In scenario 2, the role of Tx and Rx of the primary link is switched so that STA_1 and AP_1 become the Rx and Tx, respectively.

Figure 3.10(a) and (b) show the throughput performance of the primary link due to the interference in Scenario 1 and 2, respectively. During the first 30 seconds, the interfering link was not active yet as indicated by the stable throughput value. At $t = 30$ s, STA_2 started copying some huge files from the USB attached to AP_2.

In Scenario 1, the interference results in a significant degradation in the throughput (it reaches up to 0 Mbps). The throughput value remains low

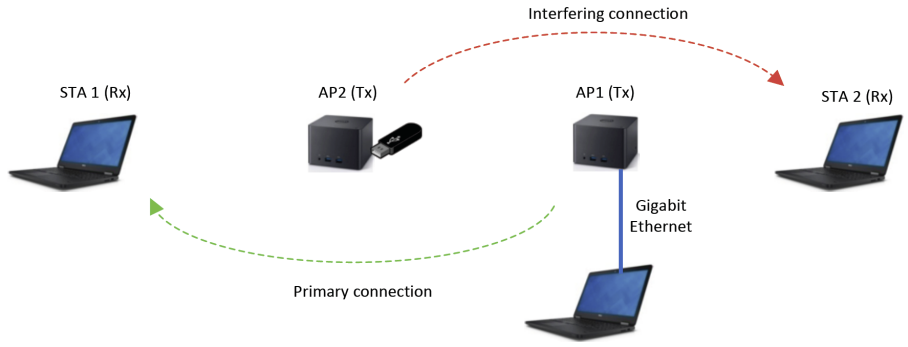

Figure 3.9: Co-channel interference scenario 2

for most of the time and can not recover to 900 Mbps as it before the interference was introduced. It is because AP_2 transmits in the opposite direction of STA_1 so that STA_1 can not hear the transmission between AP_2 and STA_2. It causes packet collisions at AP_1. The collision keeps occurring as both Tx in the primary and interfering link (STA_1 and AP_2) can not hear each other's transmission. This deafness effect is a result of the directional communication in 60 GHz.

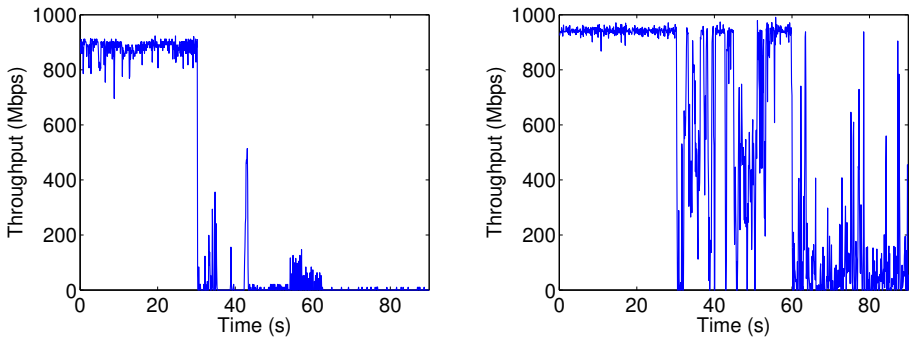

(a) Scenario 1 (b) Scenario 2

Figure 3.10: Throughput performance due to co-channel interference

Meanwhile, in Scenario 2, the throughput degradation is not as significant as that in Scenario 1. The throughput fluctuates, but 900 Mbps throughput can still be achieved in some period during the moment of interference. It is because AP_2 transmits in the direction of STA_1 (Tx) so that STA_1 can hear the transmission of interfering link. Therefore, in this scenario, packet collision occurs less frequently if compared to that in Scenario 1. Both Tx in the primary and interfering links contend for the channel access. In IEEE 802.11ad, the channel contention during the data transmission interval occurs on Contention Based Access Period (CBAP). When using different

channels, no throughput degradation was observed.

3.3 Human Blockage Effect Measurement

We performed three following measurement scenarios to represent the both transient and permanent blockage caused by the human activities in LOS and NLOS 60 GHz environments.

3.3.1 Scenario 1. Transient Blockage

In Scenario 1, the effect of transient human blockage on the link quality performance is observed. The blockage is introduced by the presence of a human walking across a 60 GHz link in a LOS environment. We used a real human body as a blockage model in which the model walked with typical human walking speed. When walking across the link, the human body temporarily blocks the link and thus causes received signal attenuation for a short duration. As soon as the human moves away from the link, STA and AP automatically try to recover the link quality by re-aligning their beam pair.

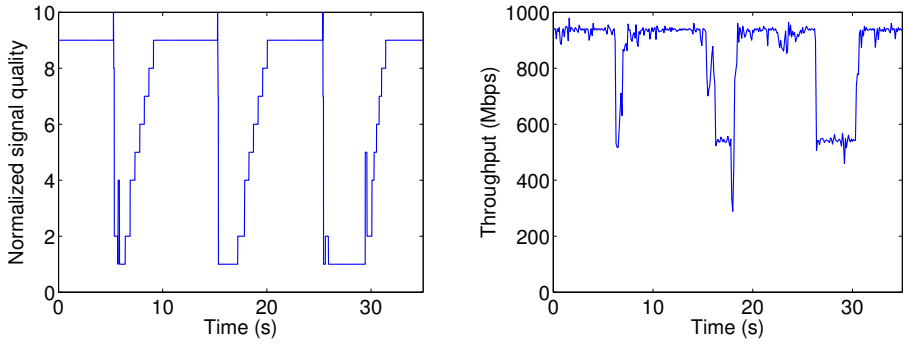

(a) Signal quality (b) Throughput

Figure 3.11: Scenario 1 measurement results at $d = 3\,\mathrm{m}$

Figure 3.11(a) and (b) respectively describe the signal quality and throughput performance against the temporary human blockage at $d = 3\,\mathrm{m}$. Three potholes with the interval of approximately 10 s in both figures indicate the moment when the human crossing the link for three times during 35 s observation period. During the obstruction moment, both signal quality and throughput suffer degradation as indicated by the temporary disruption of both parameters. In Figure 3.11(a), it is shown that the signal quality rises from 9 to 10 right before it decreases significantly to 1. It is highly likely because when the human approaches the link at $d = 3\,\mathrm{m}$, human body reflects the beam and thus focuses the beam pair between STA and AP.

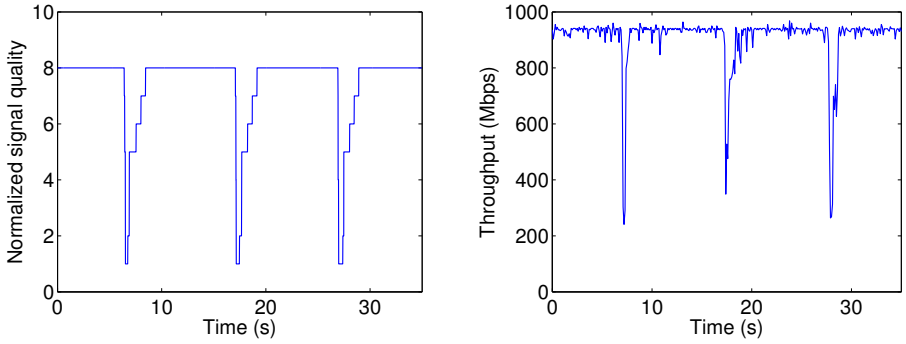

(a) Signal quality (b) Throughput

Figure 3.12: Scenario 1 measurement results at $d = 7\,\mathrm{m}$

Hence, the beam becomes more directive so that the received signal quality increases from 9 to 10 for a short period before it falls to 1 as the human body completely blocks the beam. After the human moves away from the link, the signal quality recovers from 1 to 9 within a few second. During the disruption moment, the throughput also decreases from above 900 Mbps to approximately 500 Mbps and returns to above 900 Mbps after the human moves away from the LOS path.

When d increases to 7 m, the signal quality and throughput performance also suffer the temporary disruption, as shown in Figure 3.12. At this distance, the average throughput falls drastically from above 900 Mbps to approximately 250 Mbps. However, the duration of disruption in the case of $d = 7\,\mathrm{m}$ is shorter than that in the case of $d = 3\,\mathrm{m}$.

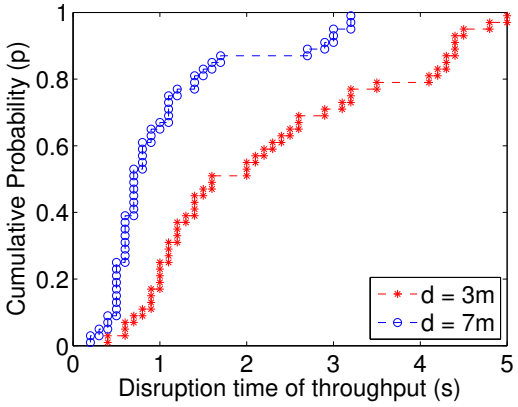

Figure 3.13: CDF of throughput disruption time in Scenario 1

Figure 3.13 depicts the Cumulative Distribution Function (CDF) of throughput disruption time due to the transient human blockage. The graph con-

firms that the closer the distance between two communicating STAs, the longer the average shadowing duration due to the human body. Note that the obstacle is presented in the middle of the distance between two STA and AP. Shortening the distance between STA and AP makes the distance between STA/AP and the obstacle closer. At the closer distance, the beamwidth of STA/AP is not wide enough if compared to the area of the human body as an obstacle. It also limits the searching space when two communicating STAs try to perform beam switching. Hence, it prolongs the time to recover. Besides, the shadowing duration of a blockage event also depends on the velocity and size of the blockers [19]. The average throughput disruption time in case of $d = 3\,\text{m}$ and $d = 7\,\text{m}$ are 2.166 s and 1.036 s, respectively. Due to the short-period link disruption, the blockage in this scenario is categorized as short-time blockage.

3.3.2 Scenario 2. Permanent Blockage With Only LOS Path

In Scenario 2, the effect of permanent human blockage on the link quality performance in a LOS environment is observed. The permanent blockage is represented by the presence of a human standing in between the STA and AP for a long duration as depicted in Figure 3.14. The blockage was presented by the human body front facing the STA or AP. Since there is only a LOS transmission path, two communicating STAs can not find any other alternative transmission path through the reflection although automatic beam switching has been performed. Consequently, the link suffers a long-term disruption.

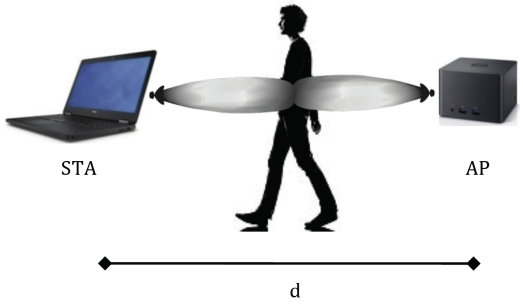

Figure 3.14: Human blockage in Scenario 2

The signal quality and throughput behavior of this scenario at $d = 3\,\text{m}$ are depicted in Figure 3.15 (a) and (b), respectively. At $t = 7\,\text{s}$, the human started blocking the link. During the obstruction, the signal quality falls drastically from 9 to 2. Meanwhile, the throughput performance does not drop significantly as the link can still achieve the average throughput of approximately 770 Mbps during the blockage. However, both signal quality and throughput could not recover to its initial condition during the presence

of the obstacle.

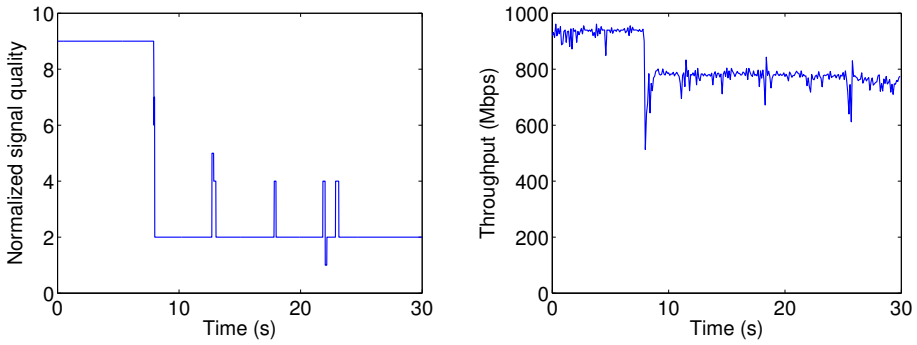

(a) Signal quality (b) Throughput

Figure 3.15: Scenario 2 measurement results at $d = 3\,\text{m}$

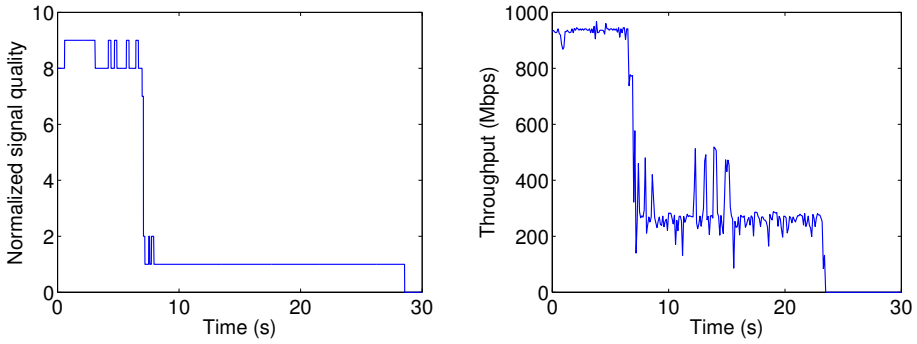

(a) Signal quality (b) Throughput

Figure 3.16: Scenario 2 measurement results at $d = 7\,\text{m}$

At $d = 7\,\text{m}$, the permanent human blockage also degrades the signal quality and throughput as shown in Figure 3.16(a) and (b), respectively. At this distance, the throughput degradation is more significant if compared to that at $d = 3\,\text{m}$. The throughput falls from above 900 Mbps to approximately 250 Mbps due to the presence of human body. It remains low until finally reaches 0 Mbps at $t = 23.4\,\text{s}$, indicating that the link is disconnected. At this distance, the human blockage causes the received signal level falls below the receiver sensitivity requirement specified by the MCS. Consequently, the link is automatically disconnected. The duration when the signal quality starts decreasing due to the presence of the obstacle until the moment when the link is disconnected is denoted as the disconnection time (t_{DC}). From the measurement at $d = 7\,\text{m}$, the average t_{DC} is **16.329 s**.

In general, the blockage in this scenario causes permanent degradation in

both signal quality and throughput performances. As the distance increases, this type of blockage can potentially break the link due to the received signal power insufficiency. Therefore, the blockage in this scenario is categorized as a long-term blockage.

3.3.3 Scenario 3. Permanent Blockage With Alternative NLOS Path

Besides LOS environment, we also observed the effect of permanent human blockage on the link quality performance in an NLOS link environment. The measurement scenario is depicted in Figure 3.17. STA and AP were placed in the distance of 1 m away from the wall. The wall acting as a reflector will reflect the beam to create an alternative NLOS transmission path in case the LOS transmission path is blocked.

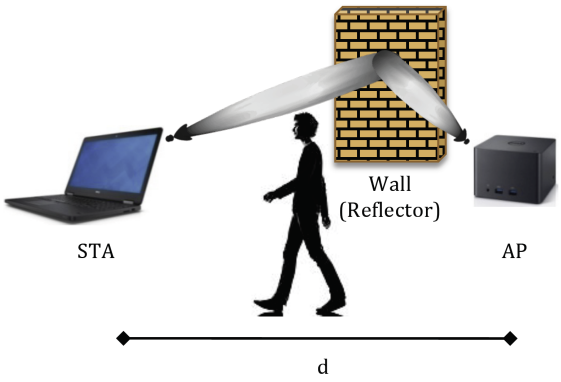

Figure 3.17: Human blockage in Scenario 3

Figure 3.18(a) and (b) respectively show the signal quality and throughput behavior of this scenario at $d = 3$ m. Following the presence of human body, the signal quality only decreases from 9 to 4 and fluctuates between 4 and 6. However, the throughput performance is not highly affected by the blockage. As shown in Figure 3.18(b), the average throughput is above 900 Mbps for most of the time during the blockage. It decreases to 600–700 Mbps within short duration for several times. When human body obstructs the LOS transmission path, STA and AP automatically perform beam switching and take advantage of the signal reflected from the wall to establish an alternative NLOS transmission path. Therefore, the signal quality does not decreases significantly and the throughput can recover faster in comparison to that in Scenario 2.

The signal quality and throughput behavior at $d = 7$ m are shown in Figure 3.19(a) and (b), respectively. At this distance, the throughput disruption due to the presence of the human body is shorter and less significant when compared to that at $d = 3$ m. Moreover, during the blockage event, the

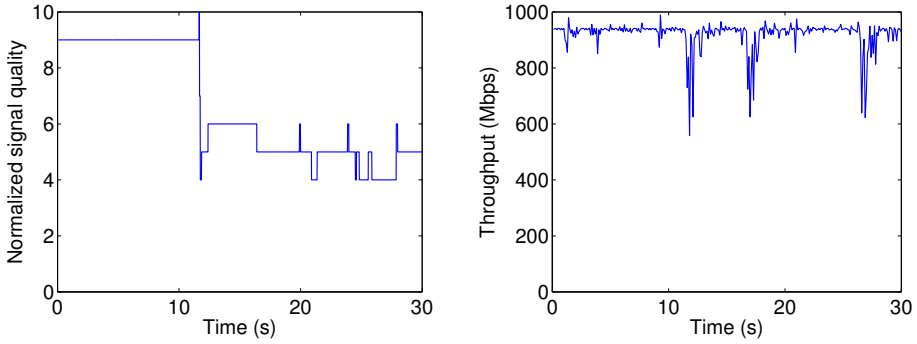

(a) Signal quality (b) Throughput

Figure 3.18: Scenario 3 measurement results at $d = 3\,\mathrm{m}$

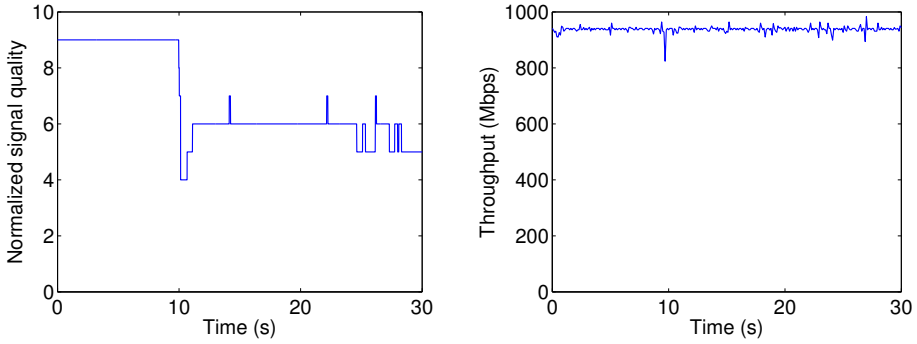

(a) Signal quality (b) Throughput

Figure 3.19: Scenario 3 measurement results at $d = 7\,\mathrm{m}$

throughput values tend to remain stable with the value of above 900 Mbps. It is slightly different from that at $d = 3\,\mathrm{m}$, in which the throughput fluctuates for several times during the presence of the obstacle. It is because, in the closer distance, the presence of human body still affects the beam of NLOS path. Consequently, the signal quality and throughput slightly fluctuate during the blockage event. As the distance between STA/AP and the obstacle increases, the presence of human body has less impact on the reflected beam.

The first-order reflection reduces the received signal level by approximately 10 dB [14]. The reduction of the received signal level leads to the re-adjustment of the MCS used. When communicating via LOS path, it is likely that the connection use the highest MCS so that the maximum data rate can be achieved. On the contrary, in the case of transmission via NLOS path, the link might use lower MCS due to the decreasing of received signal level. It results in lower achievable data rate. However, since we can

only observe the data rate up to 1 Gbps, the differences between throughput performance in LOS and NLOS transmission path can not be observed.

When the human body obstructs the LOS link, the communicating STAs try to re-adjust their beam pair for achieving higher signal quality. Thanks to the reflector, the communicating STAs can find an alternative beam pair through the reflected signal path. Although the signal quality decreases for a long period, the throughput performance can still be maintained. Since the disruption of throughput performance only occurs within a short period, the blockage in this scenario is categorized into the short-term blockage.

3.3.4 TCP and UDP Throughput

Besides using TCP traffic, we also conducted measurements of human blockage using User Datagram Protocol (UDP) traffic. The UDP traffic is generated by Iperf3 with the same configuration as shown in Figure 3.3. The parameters used in the TCP throughput measurement are shown in Table 3.2. Datagram is a transfer unit of UDP, including the data payload. We experimented with the transient blockage in Scenario 1 and the permanent blockage in Scenario 2 at $d = 7$ m.

Bandwidth	1 Gbps
Datagram Size	1470 Bytes (default)

Table 3.2: UDP throughput measurement parameter

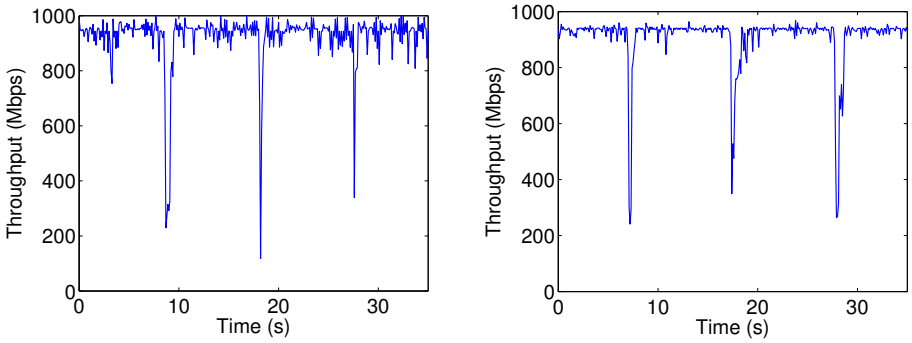

(a) UDP traffic (b) TCP traffic

Figure 3.20: Throughput performance during transient blockage

Figure 3.20(a) and (b) show the UDP and TCP throughput performances, respectively, in the case of transient blockage. Meanwhile, the UDP and TCP throughput performances in the case of permanent blockage are shown in Figure 3.21(a) and (b), respectively. The only difference between the UDP and TCP traffic is that the UDP throughput is slightly more fluc-

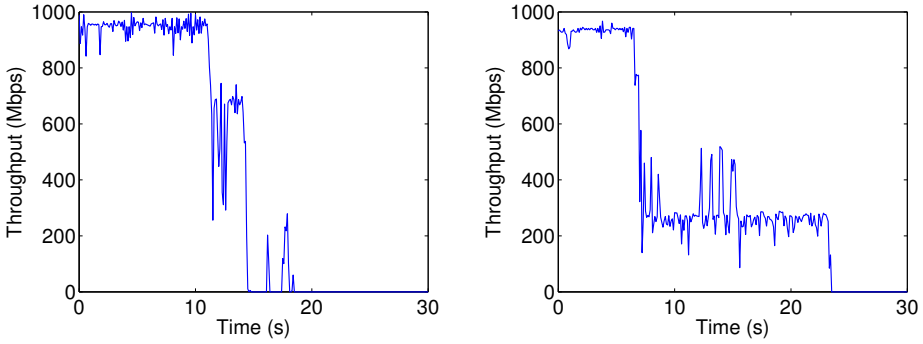

(a) UDP traffic (b) TCP traffic

Figure 3.21: Throughput performance during permanent blockage

tuative compared to the TCP throughput, especially during the absence of the obstacle. UDP is an unreliable protocol which does not guarantee that the packets sent will reach the destination. When there is a packet loss, the sender keeps transmitting the packet without adjusting the sending rate and thus causes a network congestion. The more frequent the congestion occurs, the higher the packet losses. On the other hand, in TCP, the sender can detect whether there is a packet loss during the transmission and will reduce its sending rate when detecting the packet loss. It prevents the congestion that leads to another packet loss in the next transmission. Therefore, the TCP throughput is slightly more stable than the UDP throughput. Nevertheless, in general, the results show the similarity of UDP and TCP throughput behaviour against the transient and permanent blockages.

Chapter 4

Human Blockage Characterization

In Chapter 3, we observed that the each blockage type differently affects the link performance. Therefore, each blockage type must be treated differently to minimize the duration of link disruption during the blockage event. Based on the link disruption duration, we categorize the blockage into two categories: **(i) short-term blockage** and **(ii) long-term blockage**. A short-term blockage can be caused by either the temporary blockage due to human crossing the link (Scenario 1) or when the communicating STAs can find an alternative NLOS transmission path following the permanent blockage (Scenario 3). Those conditions lead to the temporary link disruption. On the other hand, a long-term blockage is caused by the permanent human blockage in a LOS environment (Scenario 2). In this case, the communicating STAs can not establish any alternative transmission path following the blockage event and thus cause a long-term link disruption.

In this chapter, the blockage characterization method which is based on the changes of signal quality parameter is explained. We design a reactive algorithm for characterizing the blockage and implement it in a COTS 60 GHz device. Following that, we define the appropriate action to be taken in each scenario to circumvent the link outage due to blockages. A handover mechanism between the 60 GHz access points is proposed to overcome the long-period link disruption due to the long-term blockage.

4.1 Signal Quality Analysis

To characterize the blockage, we analyze the changes in the signal quality parameter during a blockage event. Figure 4.1 depicts the example of signal quality behavior when a transient blockage in Scenario 1 occurs. Upon the presence of an obstacle in between the link, the signal quality immediately decreases to a certain level. The degradation of signal quality unit is denoted

as ΔSQ_D and the time required for the signal quality to decrease as much as ΔSQ_D is denoted as the drop time (t_D). In Figure 4.1, the signal quality falls from 10 to 1 within the duration of 105 ms, thus $\Delta SQ_D = 9$ and $t_D = 105$ ms.

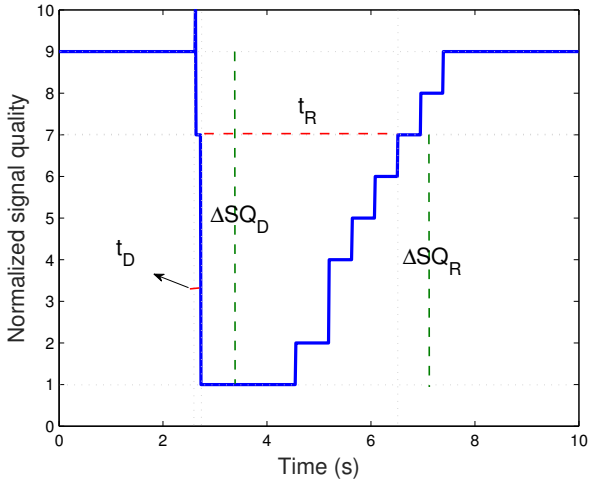

Figure 4.1: Signal quality drop and recovery in transient blockage

The signal quality remains low during the presence of human body. As soon as the human moves away from the transmission path, the communicating STAs recover the link quality by aligning their best beam pair among them. The increasing of signal quality indicates that the link is successfully recovered. ΔSQ_R is defined as how large the signal quality can improve after the blockage event. Time required for achieving ΔSQ_R is denoted as the recovery time (t_R). In Figure 4.1, it is shown that the signal quality gradually increases from 1 to 7 within 3.789 s, thus $\Delta SQ_R = 6$ and $t_R = 3.789$ s.

		$d = 3$ m	$d = 7$ m
Scenario 1	$\overline{t_D}$	197.11 ms	140.65 ms
	$t_{D_{max}}$	838 ms	513 ms
	$\overline{t_R}$	3.826 s	1.648 s
	$t_{R_{max}}$	5.726 s	2.434 s
Scenario 2	$\overline{t_D}$	232.8 ms	298.13 ms
	$t_{D_{max}}$	748 ms	952 ms
Scenario 3	$\overline{t_D}$	267.65 ms	411.27 ms
	$t_{D_{max}}$	707 ms	784 ms

Table 4.1: t_D and t_R for all blockage scenarios

Table 4.1 shows the average t_D and t_R, denoted as $\overline{t_D}$ and $\overline{t_R}$, repsectively,

for all blockage scenarios. We define the minimum $\Delta SQ_R = 6$ so that t_R becomes the time required for the signal quality to recover by at least 6 units. The larger the ΔSQ_R that the system intends to achieve, the longer t_R will be. The table only displays $\overline{t_R}$ for the blockage in Scenaro 1 as it is the only scenario that enables the signal quality to recover.

In Scenario 1, $\overline{t_D}$ and $\overline{t_R}$ are not symmetrical, in which $\overline{t_R}$ is longer than $\overline{t_D}$. It is because of the re-beamforming process. During the recovery phase, both communicating STAs try to re-align their beam pair by performing beamforming training. However, since there is a traffic presence, the beamforming training is conducted within Service Period (SP) in Data Transmission Interval (DTI). It makes the beamforming training process longer than the one conducted within Beacon Header Interval (BHI).

The maximum threshold of t_D and t_R are denoted as $t_{D_{th}}$ and $t_{R_{th}}$, respectively, indicating how long a STA has to wait for the signal quality to drop and recover, respectively. Therefore, the total decision time required by a STA to determine the blockage type equals to $t_{D_{th}} + t_{R_{th}}$.

4.2 Characterizing Blockage

Characterization of the blockage type is based on the ΔSQ_D and ΔSQ_R parameters. As explained earlier in Section 4.1, ΔSQ_D indicates how significant the signal quality falls following the presence of an obstacle. In case the blockage occurs in a LOS environment, the signal quality falls drastically since the communicating STAs can not find any backup link upon the presence of the obstacle. Consequently, the ΔSQ_D is large in the LOS environment. On the contrary, in case the blockage occurs in a NLOS environment, the communicating STAs immediately re-align their beam to find an alternative transmission path through the NLOS transmission path (if available) following the blockage event. Therefore, in this environment, the ΔSQ_D is not as significant as that in the LOS environment.

Meanwhile, ΔSQ_R indicates how much the signal quality can rise again after the blockage event. In the case of temporary human blockage, the ΔSQ_R is relatively large since the signal quality can increase to the initial condition as soon as the obstacle moves away. On the contrary, in the case of permanent human blockage, the signal quality tends to stay low during the presence of the obstacle. Hence, the ΔSQ_R is relatively small.

Figure 4.2 depicts the characteristic of ΔSQ_D and ΔSQ_R taken from 100 measurement samples for each blockage scenario at $d = 7\,\text{m}$. For this measurement, we use $t_{D_{th}} = 1\,\text{s}$ and $t_{R_{th}} = 3\,\text{s}$. Based on Figure 4.2, it can be inferred that each blockage type has unique ΔSQ_D and ΔSQ_R characteristic. For example, the blockage in Scenario 1 is indicated by a large ΔSQ_D and ΔSQ_R, while the blockage in Scenario 2 is indicated by a large ΔSQ_D and a small ΔSQ_R.

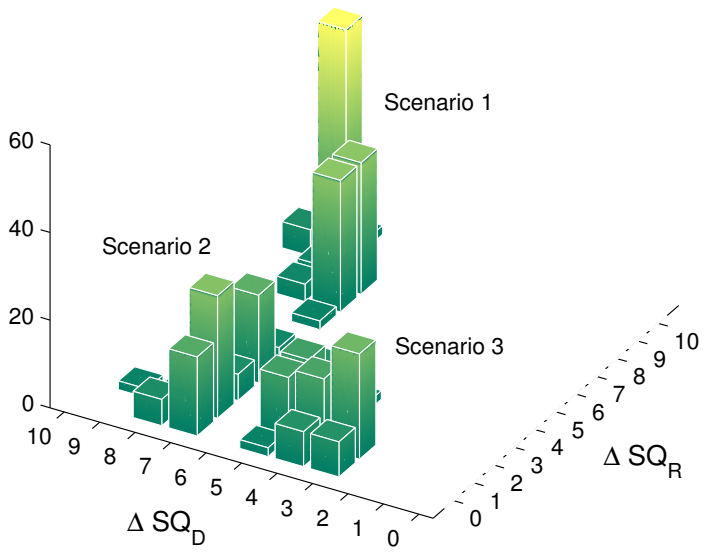

Figure 4.2: ΔSQ_D and ΔSQ_R characteristic of each blockage scenario

Scenario	ΔSQ_D (x_c)	ΔSQ_R (y_c)
1	7.72	7.64
2	7.30	1.56
3	4.06	1.20

Table 4.2: ΔSQ_D and ΔSQ_R centroid

The average values of ΔSQ_D and ΔSQ_R for all measurement scenarios are shown in Table 4.2. The average ΔSQ_D and ΔSQ_R for each scenario are then considered as the centroid constant x_c and y_c, respectively. Following that, we calculate the Euclidean Distance (ED) between the measured ΔSQ_D and ΔSQ_R defined as x and y, to the centroid x_c and y_c, as shown in Equation 4.1.

$$ED = \sqrt{(x - x_c)^2 + (y - y_c)^2} \tag{4.1}$$

By substituting x_c and y_c values specified in Table 4.2 to Equation 4.1, we get the Euclidean Distance for each blockage scenario as a function of x and y, as described in Equations 4.2–4.4.

$$ED_1(x, y) = \sqrt{(x - 7.72)^2 + (y - 7.64)^2} \tag{4.2}$$

$$ED_2(x, y) = \sqrt{(x - 7.30)^2 + (y - 1.56)^2} \tag{4.3}$$

$$ED_3(x, y) = \sqrt{(x - 4.06)^2 + (y - 1.20)^2} \tag{4.4}$$

To find the closest characteristic between the actual ΔSQ_D and ΔSQ_R with the defined blockage characteristics specified in Table 4.2, we then pick the minimum value among $ED_1(x, y)$, $ED_2(x, y)$ and $ED_3(x, y)$. The one which has the smallest Euclidean Distance is then determined as the corresponding blockage type.

Algorithm 1: Human blockage characterization

```
1: while (t ≤ t_{D_th}) do
2:     monitor ΔSQ_D
3:     x ← max(ΔSQ_D)
4: end while
5: if (x > 1) then
6:     Blockage indication
7:     while (t ≤ t_{R_th}) do
8:         monitor ΔSQ_R
9:         y ← max(ΔSQ_R)
10:    end while
11:    calculate ED_1, ED_2, ED_3
12:    b ← min(ED_1, ED_2, ED_3)
13:    if (b = ED_1  or  b = ED_3) then
14:        Short-term blockage
15:    else
16:        Long-term blockage
17:    end if
18: else
19:    No blockage
20: end if
```

The blockage characterization algorithm is described in Pseudocode 1. During the pre-defined $t_{D_{th}}$, STA monitors the ΔSQ_D for every $t = 1\,\text{ms}$ interval. If the maximum ΔSQ_D monitored is greater than 1, then there is a blockage indication. Otherwise, there is no blockage indication. We set the ΔSQ_D threshold to "1" since the signal quality might fluctuate by 1 unit in the absence of an obstacle.

After detecting the blockage indication, STA monitors the ΔSQ_R during the pre-defined $t_{R_{th}}$. We use two arrays to store each ΔSQ_D and ΔSQ_R values during $t_{D_{th}}$ and $t_{R_{th}}$, respectively. The maximum ΔSQ_D and ΔSQ_R is then defined as x and y, respectively. After getting the x and y values, ED_1, ED_2 and ED_3 are calculated. The minimum distance among ED_1, ED_2 and ED_3 is indicated as the corresponding blockage type, referred to as b. If b equals to either ED_1 or ED_3, then STA infers that a short-term blockage occurs. Otherwise, a long-term blockage occurs.

4.3 Blockage Solution

After determining the blockage type, a further action has to be taken for overcoming such blockage. The effective solution has to be determined so that the duration of link disruption can be minimized. As described in Figure 1.2, in the case of short-term blockage, STA has to keep the connection with the current AP and wait until the signal quality recovers. The relay or handover solution is not suitable for solving the short-term blockage as it causes unnecessary delay during the handover process.

On the other hand, in the case of long-term blockage, STA has to perform handover to another AP so that the long-period link disruption can be avoided. Maintaining the connection with the current AP causes permanent throughput degradation. Although the handover solution will introduce some delay, this solution is considered to be better than maintaining the connection with the current AP, regarding throughput performance.

We choose the handover approach because our wireless docking system does not support the relay or FST mechanism. Moreover, since the communication range of 60 GHz is short, it is likely that multiple APs are placed within a few meters in an environment. Therefore, the handover between APs is feasible for resolving the long-term blockage.

4.3.1 Handover in Wireless Docking System

In the cellular communication system, the term handover refers to switching the connection of Mobile Station (MS) from one Base Station (BS) to another BS. Usually, the handover in the cellular system is resulting from the user mobility. In general, there are three types of handover in mobile communication: hard handover, soft handover, and softer handover [40]. In the hard handover or so-called "Break Before Make" mechanism, a MS releases the connection with the existing BS before making a new connection with another BS. Meanwhile, in soft handover and softer handover, a MS has established a new connection with another BS before releasing the connection with the current BS. Thus, it is known as "Make Before Break" mechanism.

In this work, we use the hard handover principle since the STA can not establish more than one connection at a time. It involves the three following phases: (1) Disassociation with the current AP, (2) Finding the available alternative AP and (3) Association with the new AP. After detecting a long-term blockage, the STA is forced to disconnect from the current or primary AP. The disassociation process takes some time to complete. Once the STA is disconnected from the primary AP, it immediately scans all available APs. Upon detecting at least one alternative AP on its scanning list, the STA immediately attempts to associate with such AP. After a new connection has been established, the STA will be able to send/receive the traffic to/from the connected AP.

4.3.2 Handover Performance

We performed the measurement to observe the handover performance in terms of the time delay. The measurement setup consists of one laptop acting as a STA and two docking stations that serve as two APs as depicted in Figure 4.3. The first AP is a Primary AP, which suffers a link disruption due to the long-term blockage. The second AP is an Alternative AP of which the STA switches to following the long-term blockage indication. During the measurement, the signal quality and throughput parameters were recorded. Each AP is connected to an additional laptop generating TCP traffic by using Iperf3. The distance between the STA and each AP is 3 m. The permanent human blockage (Scenario 2) is introduced, in which a person is standing in between the STA and Primary AP during the measurement duration. In this measurement, we use $t_{D_{th}} = 1$ s and $t_{R_{th}} = 3$ s.

Figure 4.3: 60 GHz handoff measurement setup

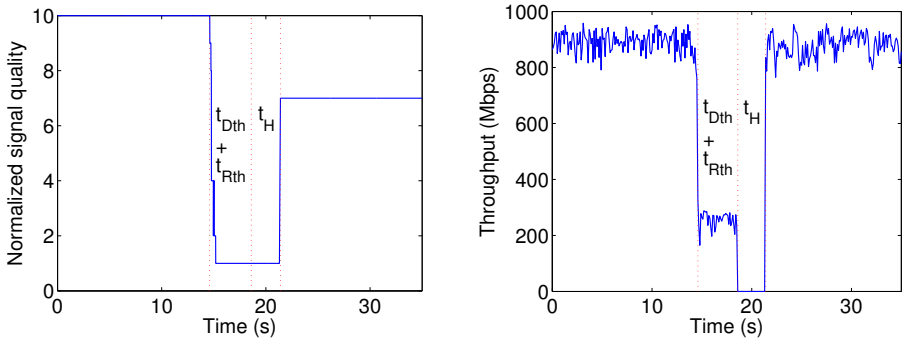

(a) Signal quality

(b) Throughput

Figure 4.4: Link quality performance during handover

The example of signal quality and throughput behavior during the handover process are described in Figure 4.4(a) and (b), respectively. In Figure

4.4(a), the signal quality can not recover to 10 after the handover process because of the suboptimal beam pair between the STA and Secondary AP. The position of Secondary AP which is slightly behind the STA results in lower directivity gain. Hence, the maximum signal quality can not be achieved. However, the link can still achieve the maximum throughput of around 900 Mbps. Time gap in both graphs indicates the moment during blockage and handover process. The total time required by a STA to complete the handover process consists of:

1. **Decision time**: time required by a STA to determine the type of blockage. It consists of $t_{D_{th}}$ and $t_{R_{th}}$ as defined in the algorithm. In this case, the decision time equals to 4 s.

2. **Handover time**: time required by a STA to complete the handover process, denoted as t_H. In this phase, the STA performs three steps of handover procedure as explained in Section 4.3.1.

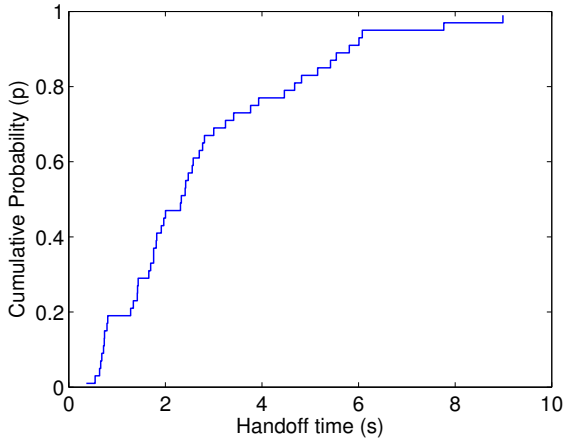

Figure 4.5: CDF of the handover time

Figure 4.5 describes the empirical CDF of the handover process duration. From the measurement results, the average t_H is **2.749 s**. t_H time component can not be reduced since it is the nature of our wireless docking system. Therefore, the only way to decrease the total gap time is by reducing the decision time component ($t_{D_{th}}$ and $t_{R_{th}}$) in the algorithm.

It has been shown that the handover process is costly in terms of the delay performance. Nevertheless, in the case of long-term blockage, it is still better to perform handover rather than to suffer the long-period link disruption. On the other hand, in the case of short-term blockage, the handover is not an effective solution because the disruption time due to the short-term blockage, as shown in Figure 3.13, is shorter than the time required for performing the handover process. Therefore, in this case, performing handover will cause an unnecessary delay.

Chapter 5

Evaluation

In this chapter, the duration of link disruption due to the human blockage is evaluated. Detecting the correct blockage type is crucial since the incorrect blockage detection leads to the longer disruption period. We evaluate the detection accuracy of the system through the measurement. Based on the duration of link disruption and the accuracy of blockage-type detection, the optimum decision time to identify the blockage type is obtained. Following that, the optimum decision time is applied to the algorithm and used to evaluate the detection accuracy against various Tx–Rx distances.

5.1 Disruption Time due to Blockage

Based on the observation of throughput performance during the blockage events, we derive the mathematical equation to determine the disruption time due to each blockage type. In the calculation, we assume that the throughput equals to 0 Mbps during the disruption period. Therefore, the term "outage duration" is used to represent the moment during link disruption. We evaluate the link outage duration resulting from both short-term and long-term blockage.

5.1.1 Outage Duration of Short-term Blockage

In the transient blockage (Scenario 1), the communicating STAs try to recover the link quality within $t_{R_{th}}$. Note that this blockage is characterized by a large ΔSQ_R. Long $t_{R_{th}}$ gives the STA enough time to observe such large ΔSQ_R so that the short-time blockage can be detected correctly. Therefore, the outage duration when the STA correctly detects the short-term blockage ($t_{O_{C(STB)}}$) equals to $t_{R_{th}}$, as indicated in Equation 5.1 and Figure 5.1.

$$t_{O_{C(STB)}} = t_{R_{th}} \tag{5.1}$$

$$t_{O_{F(STB)}} = t_{R_{th}} + t_H \tag{5.2}$$

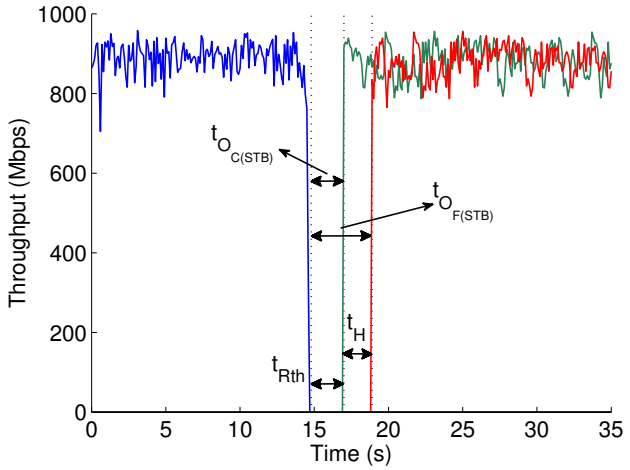

Figure 5.1: Outage duration due to short-term blockage

However, if $t_{R_{th}}$ is set too small, the STA will not have enough time to observe a large ΔSQ_R. The STA might have detected a transient blockage as a long-term blockage before the signal quality could recover. Consequently, the STA will trigger an unnecessary handover process. As discussed in Section 4.3.2, the handover process in our wireless docking system takes t_H to complete in which the throughput equals to 0 Mbps during this period. Therefore, the link outage resulting from the false detection when detecting the short-term blockage ($t_{O_{F(STB)}}$) occurs during $t_{R_{th}}$ and t_H, as indicated in Equation 5.2 and Figure 5.1.

5.1.2 Outage Duration of Long-term Blockage

If the STA detects the long-term blockage correctly, the link outage is mainly because of the handover process. Therefore, the outage duration when the system correctly detects a long-term blockage ($t_{O_{C(LTB)}}$) depends on $t_{R_{th}}$ and t_H, as indicated in Equation 5.3 and Figure 5.2.

$$t_{O_{C(LTB)}} = t_{R_{th}} + t_H \tag{5.3}$$

$$t_{O_{F(LTB)}} = t_{DC} \tag{5.4}$$

On the other hand, if the long-term blockage is incorrectly detected as the short-term blockage, the STA does not trigger the handover process. It makes the link suffer a long-term link outage. We assume that the link outage occurs until the link is automatically disconnected due to the received signal power insufficiency, which is referred to as the disconnection time (t_{DC}) as explained in Section 3.3.2. Therefore, the outage duration resulting from the incorrect detection when detecting the long-term blockage ($t_{O_{F(LTB)}}$) equals to t_{DC} as depicted in Figure 5.2 and Equation 5.4.

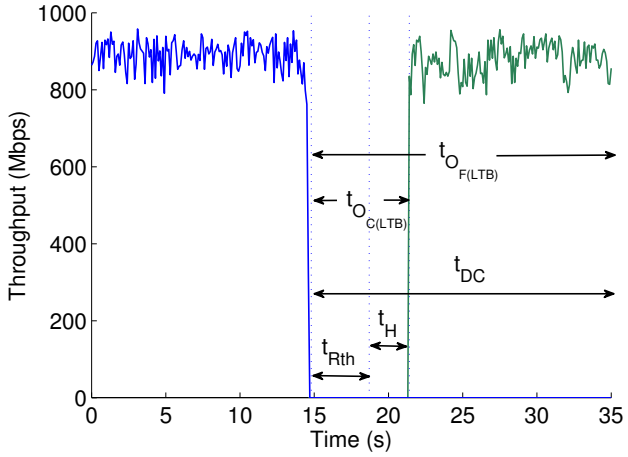

Figure 5.2: Outage duration due to long-term blockage

Handoff time (t_H)	2.749 s
Disconnection time (t_{DC})	16.329 s

Table 5.1: t_H and t_{DC} parameter

Table 5.1 shows the average t_H and t_{DC} obtained from the experiments. By substituting t_H and t_{DC} indicated in Table 5.1 to Equations 5.1–5.4, the outage duration for each blockage decision possibility is obtained as shown in Equations 5.5–5.7.

$$t_{O_{C(STB)}} = t_{R_{th}}\ s \tag{5.5}$$

$$t_{O_{F(STB)}} = t_{O_{C(LTB)}} = 2.749 + t_{R_{th}}\ s \tag{5.6}$$

$$t_{O_{L(LTB)}} = 16.329\ s \tag{5.7}$$

5.2 Detection Accuracy

As discussed in Section 5.1, the incorrect detection of the blockage type prolongs the outage duration. Therefore, the detection accuracy is important as the detection result will determine the next action to be taken. In this section, the accuracy in detecting the blockage type is evaluated.

We evaluated the detection accuracy of short-term blockage (A_{STB}) and long-term blockage (A_{LTB}) through the measurement. For each blockage type, we performed 100 measurements. The number of accurate blockage detection divided by the total number of measurements indicates the accuracy. The values of $t_{D_{th}}$ and $t_{R_{th}}$ are varied to observe their effects on the detection accuracy. While keeping $t_{R_{th}}$ fixed, we modified $t_{D_{th}}$, and vice versa.

$t_{D_{th}}$	$t_{R_{th}}$	A_{STB}	A_{LTB}
250 ms		88 %	56 %
500 ms	1 s	68 %	88 %
750 ms		76 %	92 %
250 ms		96 %	73 %
500 ms	**3 s**	**97 %**	**96 %**
750 ms		99 %	97 %
250 ms		100 %	72 %
500 ms	6 s	96 %	92 %
750 ms		100 %	96 %

Table 5.2: Detection accuracy for various $t_{D_{th}}$

Table 5.2 shows the accuracy performance for various $t_{D_{th}}$ values. Firstly, we picked $t_{R_{th}}$ of 3 s and experimented with several $t_{D_{th}}$ values: 250 ms, 500 ms and 750 ms. We performed 100 measurements of transient human blockage (Scenario 1) and permanent human blockage (Scenario 2) to measure A_{STB} and A_{LTB}, respectively. The results show that reducing $t_{D_{th}}$ from 1 s to 250 ms does not significantly influence A_{STB} since it tends to remain constant above 95%. However, lowering $t_{D_{th}}$ to 250 ms reduces A_{LTB} to 73%. It is because when $t_{D_{th}}$ is too short, the station does not have enough time to detect the large magnitude of ΔSQ_D in the case of the permanent blockage in Scenario 2. As discussed in Section 4.2, the blockage in Scenario 2 is characterized by a large ΔSQ_D. Instead, during the short $t_{D_{th}}$, STA might only detect a small ΔSQ_D which is the characteristic of the blockage in Scenario 3. In this case, the long-term blockage (Scenario 2) is incorrectly detected as the short-term blockage (Scenario 3).

In addition, we also performed the measurement using $t_{R_{th}} = 1$ s and 6 s. This time, we only performed 25 measurements for each $t_{D_{th}}$ and $t_{R_{th}}$ pair. When $t_{R_{th}} = 6$ s is used, A_{STB} and A_{LTB} behaviour is similar than that when $t_{R_{th}} = 3$ s is used. However, when $t_{R_{th}} = 1$ s is used, A_{STB} decrease in several $t_{D_{th}}$ values (500 ms and 750 ms). It is because the system can only detect a small ΔSQ_R during a short $t_{R_{th}}$ period. Consequently, the short-term blockage will be detected as the long-term blockage that leads to the decreasing of A_{STB}. A special case occurs when $t_{D_{th}} = 250$ ms and $t_{R_{th}} = 1$ ms are used. A_{STB} is relatively high because the system only detects a small ΔSQ_D as well as ΔSQ_R. In this case, the characteristic of ΔSQ_D and ΔSQ_R is very close to the characteristic of blockage in Scenario 3. Most of the blockages in Scenario 1 or Scenario 2 are detected as a blockage in Scenario 3 (short-term blockage). Therefore, A_{STB} is high while A_{LTB} is low.

Comparing the outage duration in Equation 5.5–5.7, it is shown that $t_{O_{L(LTB)}}$ contributes the longest outage duration among others. Allowing

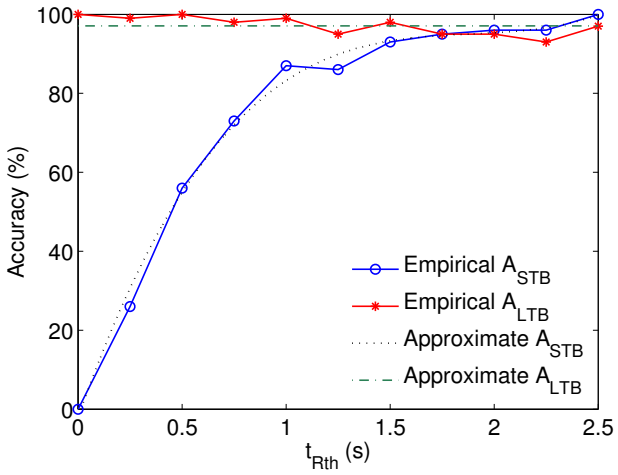

Figure 5.3: Detection accuracy vs $t_{R_{th}}$

the incorrect detection of a long-term blockage results in the significant downtime. Therefore, we choose 500 ms as the optimum $t_{D_{th}}$ because it is the shortest $t_{D_{th}}$ that can still provide high A_{LTB} as well as A_{STB}. Furthermore, as shown in Table 4.1, $\overline{t_D}$ for the blockage in Scenario 1, 2 and 3 are 140.54 ms, 298.13 ms and 411.27 ms, respectively. Therefore, setting $t_{D_{th}}$ to 500 ms still enables the system to detect ΔSQ_D for all blockage scenarios with high accuracy. This $t_{D_{th}}$ value is used in the next measurement to find the optimum $t_{R_{th}}$.

Figure 5.3 shows the detection accuracy performance for various $t_{R_{th}}$ values. For this measurement, we used a fixed $t_{D_{th}}$ of 500 ms. It is shown that A_{STB} highly depends on the $t_{R_{th}}$. Lowering $t_{R_{th}}$ leads to the decreasing of A_{STB}. It is because when $t_{R_{th}}$ is too short, the system does not have enough time to observe the large ΔSQ_R. Consequently, the system has hastily inferred the long-term blockage before the signal quality could recover, as explained in Section 5.1.1. We performed polynomial curve fitting to find the approximate relation between A_{STB} and $t_{R_{th}}$. By doing so, we found that the relation between A_{STB} and $t_{R_{th}}$ for $0 \leq t_{R_{th}} \leq 2.5$ s fits to the 3rd polynomial (cubic) equation as shown in Equation 5.8.

$$A_{STB}(t_{R_{th}}) = 0.138(t_{R_{th}})^3 - 0.78(t_{R_{th}})^2 + 1.495(t_{R_{th}}) - 0.021 \tag{5.8}$$

$$A_{LTB} = 97.08\% \tag{5.9}$$

On the other hand, A_{LTB} is not affected by the variation of $t_{R_{th}}$ as A_{LTB} tends to be constant above 90% for various $t_{R_{th}}$. A_{LTB} is approximated by averaging A_{LTB} values during $0 \leq t_{R_{th}} \leq 2.5$ s, as shown in Equation 5.9.

5.3 Optimum Decision Time

The total decision time consists of $t_{D_{th}}$ and $t_{R_{th}}$ components, in which $t_{R_{th}}$ contributes the most significant waiting time. As shown in Figure 5.3, the higher the $t_{R_{th}}$, the higher accuracy of blockage detection, especially the short-term blockage. Lowering the $t_{R_{th}}$ results in the low detection accuracy, especially A_{STB}. However, increasing $t_{R_{th}}$ makes the waiting time longer. Therefore, there is a trade-off between the decision time and the detection accuracy. Choosing an optimum $t_{R_{th}}$ value is critical so that the waiting time can be minimized while the high detection accuracy can still be maintained. In this section, the optimum $t_{R_{th}}$ is obtained by calculating the total outage duration due to the blockage.

The total outage duration ($t_{O_{tot}}$) in a blockage event is formulated in Equation 5.10. It is determined by the probability that the short-term and long-term blockage will occur (p_{STB} and p_{LTB}), the accuracy in detecting each blockage type (A_{STB} and A_{LTB}) and the outage duration of each blockage type ($t_{O_{C(STB)}}$, $t_{O_{F(STB)}}$, $t_{O_{C(LTB)}}$ and $t_{O_{F(LTB)}}$). Since there are only two possible decisions: short-term and long-term blockage, then $p_{LTB} = 1 - p_{STB}$.

$$\begin{aligned} t_{O_{tot}} = p_{STB}(A_{STB}.t_{O_{C(STB)}} + (1 - A_{STB}).t_{O_{F(STB)}}) + \\ p_{LTB}(A_{LTB}.t_{O_{C(LTB)}} + (1 - A_{LTB}).t_{O_{F(LTB)}}) \end{aligned} \tag{5.10}$$

By subsituting p_{LTB} = 1 - p_{STB}, $t_{O_{C(STB)}}$, $t_{O_{F(STB)}}$, $t_{O_{C(LTB)}}$, $t_{O_{F(LTB)}}$, A_{STB} and A_{LTB} from Equation 5.5–5.9, respectively, to Equation 5.10, we will get $t_{O_{tot}}$ as a function of $t_{R_{th}}$ and p_{STB}, as shown in Equation 5.11.

$$\begin{aligned} t_{O_{tot}}(t_{R_{th}}, p_{STB}) = p_{STB}(-0.138.{t_{R_{th}}}^4 + 0.628.{t_{R_{th}}}^3 - 0.636.{t_{R_{th}}}^2 \\ + \left(\frac{0.971}{p_{STB}} - 1.596\right)t_{R_{th}} + \frac{3.146}{p_{STB}} - 0.374)\ s \end{aligned} \tag{5.11}$$

Figure 5.4 displays the relation between $t_{O_{tot}}$ and $t_{R_{th}}$ for several p_{STB} values. For the same $t_{R_{th}}$, the lower p_{STB} (higher p_{LTB}) results in the longer outage duration. It is because the outage duration due to the long-term blockage ($t_{O_{C(LTB)}}$ and $t_{O_{F(LTB)}}$) are higher than that due to the short-time blockage ($t_{O_{C(STB)}}$ and $t_{O_{F(STB)}}$). Therefore, if the long-term blockage occurs more frequently, the total outage duration will be longer.

From the graph, the optimum $t_{R_{th}}$ for each p_{STB} is achieved at the minimum $t_{O_{tot}}$. Increasing or decreasing the $t_{R_{th}}$ above or under its optimum value might result in the longer outage duration. To find the optimum $t_{R_{th}}$, we differentiate $t_{O_{tot}}$ in Equation 5.11 with respect to $t_{R_{th}}$. The optimum $t_{R_{th}}$ is obtained when $\frac{dt_{O_{tot}}}{dt_{R_{th}}} = 0$ as shown in Equation 5.12.

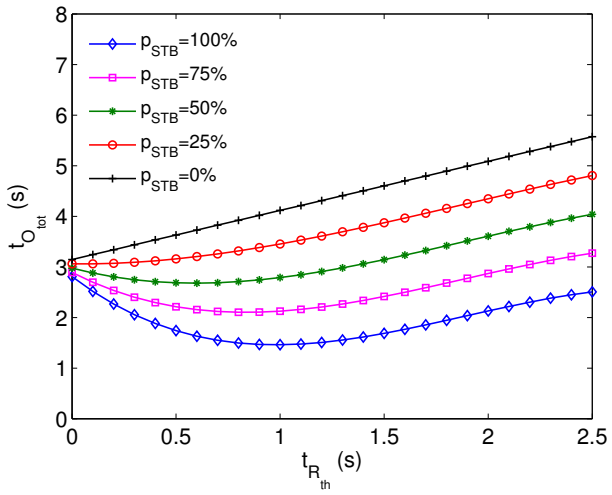

Figure 5.4: $t_{O_{tot}}$ and $t_{R_{th}}$ relation

$$\frac{dt_{O_{tot}}}{dt_{R_{th}}} = p_{STB}(-0.552.{t_{R_{th}}}^3 + 1.884.{t_{R_{th}}}^2 - 1.272.t_{R_{th}} + \frac{0.971}{p_{STB}} - 1.596) = 0 \tag{5.12}$$

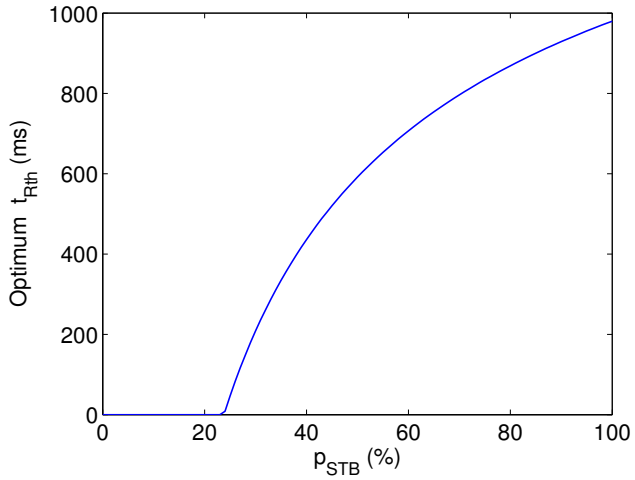

Figure 5.5: Optimum $t_{R_{th}}$ for different p_{STB}

By solving Equation 5.12, the optimum $t_{R_{th}}$ for various p_{STB} values are obtained. Figure 5.5 depicts the optimum $t_{R_{th}}$ value for all p_{STB}. In the environment where the probability of short-term blockage is relatively small ($p_{STB} \leq$ 23%), setting $t_{R_{th}}$ to 0 s minimizes the outage duration. As p_{STB}

increases, higher $t_{R_{th}}$ has to be set. The highest optimum $t_{R_{th}}$ is 980 ms reached when p_{STB} is 100 %. Therefore, the highest optimum decision time is $t_{D_{th}} + t_{R_{th}} = 500 + 980$ ms = **1480 ms**.

5.4 Detection Accuracy vs Distance

By using the optimum $t_{D_{th}}$ and $t_{R_{th}}$ obtained previously in Section 5.3, we evaluated the accuracy of blockage detection over various distances. This measurement is intended to observe the ability of the system in detecting the blockage at a long Tx–Rx distance. The measurement was conducted in an outdoor environment so that the large Tx–Rx distance can be achieved. In this experiment, the temporary blockage in Scenario 1, and the permanent blockage in Scenario 2 were performed. We use $t_{D_{th}} = 500$ ms and $t_{R_{th}} = 980$ ms.

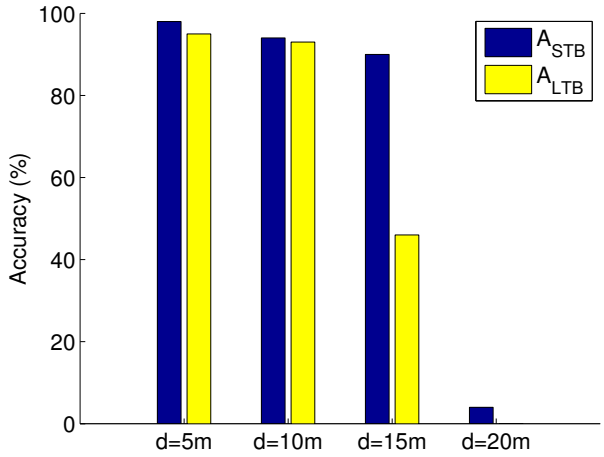

Figure 5.6: Detection accuracy for various distances

Figure 5.6 depicts the A_{STB} and A_{LTB} for various distances. It is shown that both A_{STB} and A_{LTB} are high at $d = 5$ and 10 m. When d increases to 15 m, A_{STB} is still above 90%, but A_{LTB} decreases to less than 50%. In this distance, the maximum achievable signal quality decreases to approximately 5 or 6 without the presence of any obstacle. It makes the ΔSQ_D following the presence of the obstacle less significant when compared to ΔSQ_D in the case of closer Tx–Rx distance.

As discussed in Section 4.2, the blockage in Scenario 2 has a large ΔSQ_D characteristic while the blockage in Scenario 3 has a medium ΔSQ_D characteristic. The low A_{LTB} is because the measured ΔSQ_D at $d = 15$ m has closer characteristic with the blockage in Scenario 3. Thus, it makes the long-term blockage (Scenario 2) incorrectly detected as the short-term

blockage (Scenario 3).

In the further distance ($d = 20\,\text{m}$), both A_{STB} and A_{LTB} decrease to less than 5%. In this distance, the maximum achievable signal quality decreases to approximately 2, in the absence of an obstacle. The presence of the human body causes the signal quality decreases to 1, so that most of the time, ΔSQ_D is only 1 unit. Since the algorithm ignores the blockage detection for $\Delta SQ_D \leq 1$ as explained in Section 4.2, most of the blockages are not detected by the system. This misdetection results in very low accuracy in detecting both blockage types.

Based on the results above, it can be concluded that the algorithm can detect all blockage types with the high accuracy at Tx–Rx distance up to 10 m, which is the typical operational distance for this wireless docking system.

Chapter 6

Conclusion

The 60 GHz band has emerged as a potential candidate to fulfill the desired network capacity growth as it provides large contiguous bandwidth. However, the communication in 60 GHz band suffers from higher path loss compared to that in sub-6 GHz bands. To compensate the high path loss, a highly directional antenna has to be used. The usage of a highly directional antenna and the small wavelength in 60 GHz communication make it vulnerable to human body blockage. Human activities in a 60 GHz link environment might disrupt the link and thus cause a link quality degradation.

Various human activities result in different effects on the 60 GHz link performance. Therefore, blockage characterization is necessary so that each blockage type can be treated differently to minimize the effect of link disruption. This thesis provides a human blockage characterization method that can distinguish between a temporary and permanent human blockage in both LOS and NLOS environments. The blockage characterization determines the action has to be taken to circumvent the blockage.

We categorize the human blockage into two types: short-term and long-term blockage, based on the duration of the link disruption. In the case of short-term blockage, the station has to keep the connection with the current AP. On the contrary, in the case of long-term blockage, maintaining the connection with the current AP causes long-period link disruption. To prevent this, we propose a handover mechanism between APs that is triggered following the long-term blockage indication. Our results show that the handover can maintain the continuity of transmission and avoid the long-term link disruption, although there is some interruption delay during that process.

The duration of a link disruption depends on the detection accuracy and the probability of blockage type. Incorrect detection of a blockage type aggravates the link disruption. Therefore, the accuracy in detecting the correct blockage type is important. Nevertheless, there is a trade-off between the detection accuracy and the decision waiting time. The decision time has to be as small as possible so that the station can immediately take an action

to overcome the blockage. However, reducing the decision time results in poor detection accuracy. Therefore, choosing the optimum decision time is crucial in order to minimize the waiting time while maintaining high detection accuracy. In an environment where the likelihood of short-term blockage is small, lowering the decision time minimizes the total link outage duration.

We also evaluated the effect of various Tx–Rx distances on the detection accuracy. Our results show that the system can obtain high accuracy in detecting both blockage types for the Tx–Rx distance up to 10 m, which is a typical operational distance of our device.

Besides minimizing the outage duration due to the blockage, this blockage characterization method can also be used for other purposes such as observing how frequent a certain human blockage type occurs in an area, as well as discovering the alternative transmission paths in an environment. Such information is useful to determine the optimal placement of a 60 GHz AP or the relay stations when implementing a 60 GHz network in an environment.

6.1 Future Work

Experimental studies on 60 GHz communication is still in its infancy. We have provided a first step to determine the characteristic of human blockage by using COTS 60 GHz devices. However, several hardware restrictions limit our measurements. Firstly, the signal quality is represented in a very limited resolution that complicates interpretation. Secondly, the throughput performance measurement is also limited up to 1 Gbps due to the limitation of the Gigabit Ethernet port used. It becomes a bottleneck when measuring multi-Gbps data rate provided by the 60 GHz connection.

Due to the time constraints, only the blockage effect caused by a single person was measured in this work. However, the number of persons blocking the link might affect the duration of link disruption. Therefore, observing the blockage effect due to multiple persons blocking the link simultaneously can be a future work.

Bibliography

[1] Kishor Chandra, Zizheng Cao, TM Bruintjes, R Venkatesha Prasad, G Karagiannis, Eduward Tangdiongga, HPA van den Boom, and ABJ Kokkeler. mcran: A radio access network architecture for 5g indoor communications. In *In IEEE ICC 2015 - Workshop on Fiber-Wireless Integrated Technologies, Systems and Networks (ICC'15 - Workshops 09)*., 2015.

[2] Kishor Chandra, R Venkatesha Prasad, and Ignas Niemegeers. An architectural framework for 5g indoor communications. In *2015 International Wireless Communications and Mobile Computing Conference (IWCMC)*, pages 1144–1149. IEEE, 2015.

[3] Kishor Chandra and R Venkatesha Prasad. Directional mac protocols for 60 ghz millimeter wave wlans. In *Wireless Network Performance Enhancement via Directional Antennas: Models, Protocols, and Systems*, pages 169–187. CRC Press, 2015.

[4] Jeroen Hoebeke, Gerry Holderbeke, Ingrid Moerman, Martin Jacobsson, Venkatesha Prasad, N Cempaka Wangi, Ignas Niemegeers, and S Heemstra De Groot. Personal network federations. In *Proceedings of the 15th IST Mobile & Wireless Communications Summit*. Myconos.

[5] IEEE LAN and MAN Standards Committee. *IEEE 802.11ad Standard: Wireless LAN Medium Access Control (MAC) and Physical Layer (PHY) Specifications*, volume Amendment 3 : Enhancements for Very High Throughput in the 60 GHz Band. 2012.

[6] IEEE LAN/MAN Standards Committee. Part 15.3: Wireless Medium Access Control (MAC) and Physical Layer (PHY) Specifications for High Rate Wireless Personal Area Networks (WPANs), 2009.

[7] ECMA International. Standard ECMA-387: High rate 60 GHz PHY, MAC and PALs. 2010.

[8] Sanjib Sur, Vignesh Venkateswaran, Xinyu Zhang, and Parmesh Ramanathan. 60 GHz Indoor Networking through Flexible Beams : A Link-Level Profiling. *Acm Sigmetrics*, pages 71–84, 2015.

[9] Sylvain Collonge, Gheorghe Zaharia, and Ghais El Zein. Influence of the human activity on wide-band characteristics of the 60 GHz indoor radio channel. *IEEE Transactions on Wireless Communications*, 3(6):2396–2406, 2004.

[10] Martins Jacob, Christian Mbianke, and Thomas Kürner. Human Body Blockage - Guidelines for TGad MAC development. Technical Report November, 2009.

[11] ITU-R. Attenuation by atmospheric gases. *P Series Radiowave propagation*, 10, 2013.

[12] Kishor Chandra, R Venkatesha Prasad, Ignas GMM Niemegeers, and Abdur R Biswas. Adaptive beamwidth selection for contention based access periods in millimeter wave wlans. In *2014 IEEE 11th Consumer Communications and Networking Conference (CCNC)*, pages 458–464. IEEE, 2014.

[13] Federal Communications Commission. Revision of Part 15 of the Commission's Rules Regarding Operation in the 57-64 GHz Band. Technical report, 2015.

[14] Alexander Maltsev, Roman Maslennikov, Alexey Sevastyanov, Alexey Khoryaev, and Artyom Lomayev. Experimental investigations of 60 GHz WLAN systems in office environment. *IEEE Journal on Selected Areas in Communications*, 27(8):1488–1499, 2009.

[15] IEEE 802.15 Task Group 3c. http://www.ieee802.org/15/pub/tg3c.html.

[16] Kishor Chandra, Arjan Doff, Zizheng Cao, R. Venkatesha Prasad, and Ignas Niemegeers. 60 GHz MAC Standardization: Progress and Way Forward. *2015 12th Annual IEEE Consumer Communications and Networking Conference, CCNC 2015*, pages 182–187, 2015.

[17] ITU. ITU-R M.2003 Multiple Gigabit Wireless Systems in frequencies around 60 GHz. Technical report, 2012.

[18] Thomas Nitsche, Carlos Cordeiro, Adriana B Flores, Edward W Knightly, Eldad Perahia, and I Nvited P Aper. RADIO COMMUNICATIONS IEEE 802.11ad : Directional 60 GHz Communication for Multi Gigabit-per-Second Wi-Fi. (December):132–141, 2014.

[19] Y. Ming Tsang and Ada S Y Poon. Detecting human blockage and device movement in mmwave communication system. *GLOBECOM - IEEE Global Telecommunications Conference*, 2011.

[20] A. W. Doff, K. Chandra, and R. Venkatesha Prasad. Sensor assisted movement identification and prediction for beamformed 60 GHz links.

2015 12th Annual IEEE Consumer Communications and Networking Conference, CCNC 2015, (i):648–653, 2015.

[21] A. Khfaji, R. Saadane, J. El Abbadi, and M. Belkasmi. Ray Tracing Technique based 60 GHz Band Propagation Modelling and Influence of People Shadowing. *Engineering and Technology*, 2(9):667–673, 2008.

[22] Martin Jacob, Sebastian Priebe, Alexander Maltsev, Artyom Lomayev, Vinko Erceg, and Thomas Kurner. A ray tracing based stochastic human blockage model for the IEEE 802.11ad 60 GHz channel model. *Proceedings of the 5th European Conference on Antennas and Propagation (EUCAP)*, (m):3084–3088, 2011.

[23] Carl Gustafson and Fredrik Tufvesson. Characterization of 60 GHz shadowing by human bodies and simple phantoms. *Radioengineering*, 21(4):979–984, 2012.

[24] Jonathan Lu, Daniel Steinbach, Patrick Cabrol, and Philip Pietraski-InterDigital. Modeling the Impact of Human Blockers in Millimeter Wave Radio Links. *ZTE Communications Magazine*, 10(4):23–28, 2012.

[25] Y Oguma, R Arai, T Nishio, K Yamamoto, and M Morikura. Proactive Base Station Selection Based on Human Blockage Prediction Using RGB-D Cameras for mmWave Communications. *2015 IEEE Global Communications Conference (GLOBECOM)*, pages 1–6, 2015.

[26] Sanjib Sur, Xinyu Zhang, Parmesh Ramanathan, and Ranveer Chandra. BeamSpy : Enabling Robust 60 GHz Links Under Blockage This paper is included in the Proceedings of the. *Proceedings of the 13th USENIX Symposium on Networked Systems Design and Implementation (NSDI '16)*, pages 193 —- 206, 2016.

[27] Roberto Congiu, Hossein Shokri-Ghadikolaei, Carlo Fischione, and Fortunato Santucci. On the Relay-Fallback Tradeoff in Millimeter Wave Wireless System. page 6, 2016.

[28] Kishor Chandra, R. Venkatesha Prasad, Bien Quang Niemegeers, and Ignas. Cogcell:cognitive interplay between 60ghz picocells and 2.4/5ghz hotspots in the 5g era. *IEEE Communications Magazine, Special issue on Emerging Applications, Services and Engineering for Cognitive Cellular Systems (EASE4CCS),*, 2015.

[29] Swetank Kumar Saha, Viral Vijay Vira, Anuj Garg, and Dimitrios Koutsonikolas. 60 GHz Multi-Gigabit Indoor WLANs: Dream or Reality? 2015.

[30] Thomas Nitsche, Guillermo Bielsa, Irene Tejado, and Universidad Carlos Iii. Boon and Bane of 60 GHz Networks : Practical Insights into Beamforming , Interference , and Frame Level Operation. 2015.

[31] Junaid Ansari, Nikos Perpinias, Alexander Nahring, Petri Mahonen, and Marina Petrova. Empirical characterization of mm-wave communication links in realistic indoor scenarios. *2015 IEEE Wireless Communications and Networking Conference (WCNC)*, pages 1799–1804, 2015.

[32] Adrian Loch. Millimeter-Wave Blind Spots : Mitigating Deafness Collisions Using Frame Aggregation. (mmNet), 2016.

[33] Daniel Halperin, Srikanth Kandula, Jitendra Padhye, Paramvir Bahl, and David Wetherall. Augmenting data center networks with multi-gigabit wireless links. *Sigcomm 2011*, 41(4):38, 2011.

[34] Yibo Zhu, Xia Zhou, Zengbin Zhang, Lin Zhou, Amin Vahdat, Ben Y. Zhao, and Haitao Zheng. Cutting the cord: a Robust Wireless Facilities Network for Data Centers. *Proceedings of the 20th annual international conference on Mobile computing and networking - MobiCom '14*, pages 581–592, 2014.

[35] Yibo Zhu, Zengbin Zhang, Zhinus Marzi, Chris Nelson, Upamanyu Madhow, Ben Y Zhao, and Haitao Zheng. Demystifying 60GHz outdoor picocells. *the 20Th Annual International Conference*, pages 5–16, 2014.

[36] Ljiljana Simić, Nikos Perpinias, and Marina Petrova. 60 GHz Outdoor Urban Measurement Study of the Feasibility of Multi-Gbps mm-Wave Cellular Networks. (mmNet):331–336, mar 2016.

[37] Intel Corporation. Intel® Wireless Gigabit Sink W13100 Product Brief.

[38] Intel Corporation. Intel® Tri-Band Wireless-AC 17265 Product Brief.

[39] iPerf - The TCP, UDP and SCTP network bandwidth measurement tool.

[40] William Lee. *Wireless and Cellular Communications*. McGraw-Hill, third edition, 2005.

[41] Adrian Loch, Irene Tejado, and Joerg Widmer. Potholes Ahead: Impact of Transient Link Blockage on Beam Steering in Practical mm-Wave Systems. pages 1–15, 2016.

[42] Thomas Nitsche, Adriana B. Flores, Edward W. Knightly, and Joerg Widmer. Steering with eyes closed: Mm-Wave beam steering without in-band measurement. *Proceedings - IEEE INFOCOM*, 26:2416–2424, 2015.

[43] Julian Arnold, Ljiljana Simi, Marina Petrova, and Petri Mähönen. Demo : Spectrum-Agile mm-Wave Packet Radio Implementation on USRPs. pages 5–8, 2015.

[44] Gek Hong Sim, Rui Li, Cristina Cano, David Malone, Paul Patras, and Joerg Widmer. Learning from Experience : Efficient Decentralized Scheduling for 60GHz Mesh Networks. 2016.

[45] Yuta Oguma, Takayuki Nishio, Koji Yamamoto, and Masahiro Morikura. Proactive Traffic Control based on Human Blockage Prediction using RGB-D Cameras for mmWave Communications. *IEICE Transactions on Communications*, E99B(8):1734–1744, 2016.

[46] M Ghaddar and M Nedil. Experimental Analysis of Human Body Effects on NLOS 60 GHz Propagation Channel. pages 1788–1789, 2015.

Appendix A

IEEE 802.11ad MCS

PHY	MCS	Modulation	Code Rate	Data Rate (Mbps)	Receiver Sensitivity (dBm)
Control	0	$\pi/2$-DBPSK	1/2	27.5	-78
Single Carrier (SC)	1	$\pi/2$-BPSK	1/2	385	-68
	2	$\pi/2$-BPSK	1/2	770	-66
	3	$\pi/2$-BPSK	5/8	962.5	-65
	4	$\pi/2$-BPSK	3/4	1155	-64
	5	$\pi/2$-BPSK	13/16	1251.25	-62
	6	$\pi/2$-QPSK	1/2	1540	-63
	7	$\pi/2$-QPSK	5/8	1925	-62
	8	$\pi/2$-QPSK	3/4	2310	-61
	9	$\pi/2$-QPSK	13/16	2502.5	-59
	10	$\pi/2$-16QAM	1/2	3080	-55
	11	$\pi/2$-16QAM	5/8	3850	-54
	12	$\pi/2$-16QAM	3/4	4620	-53
OFDM	13	SQPSK	1/2	693	-66
	14	SQPSK	5/8	866.25	-64
	15	QPSK	1/2	1386	-63
	16	QPSK	5/8	1732.5	-62
	17	QPSK	3/4	2079	-60
	18	16QAM	1/2	2772	-58
	19	16QAM	5/8	3465	-56
	20	16QAM	3/4	4158	-54
	21	16QAM	13/16	4504.5	-53
	22	64QAM	5/8	5197.5	-51
	23	64QAM	3/4	6237	-49
	24	64QAM	13/16	6756	-47

PHY	MCS	Modulation	Code Rate	Data Rate (Mbps)	Receiver Sensitivity (dBm)
Low Power SC	25	$\pi/2$-BPSK	13/28	626	-64
	26	$\pi/2$-BPSK	13/21	834	-60
	27	$\pi/2$-BPSK	52/63	1112	-57
	28	$\pi/2$-QPSK	13/28	1251	-57
	29	$\pi/2$-QPSK	13/21	1668	-57
	30	$\pi/2$-QPSK	52/63	2224	-57
	31	$\pi/2$-QPSK	13/14	2503	-57

Table A.1: Data rate and receiver sensitivity corresponding to MCS

Appendix B

60 GHz Experimental: Comparative Review

No	Work	DUT Hardware (60 GHz Transmitter)	Additional Receiver System	Environment	Measurement Parameters	60 GHz Issues
1	60 GHz Multi-Gigabit Indoor WLANs: Dream or Reality? [29]	COTS: Dell D5000 Docking station, Dell Latitude E7420 Laptop (Wilocity wil6210 chipset)	-	Indoor	Normalized signal quality, PHY rate, TCP throughput (iperf3)	Tx-Rx distance, Tx-Rx height difference, Link blockage, Interference
2	Potholes Ahead: Impact of Transient Link Blockage on Beam Steering in Practical mm-Wave Systems [41]	COTS: Dell D5000 Docking station, Dell Latitude E7440 Laptop	SiversIMA USRP X310	Indoor	Signal level (Volt), TCP throughput	Link blockage

No	Work	DUT Hardware (60 GHz Transmitter)	Additional Receiver System	Environment	Measurement Parameters	60 GHz Issues
3	Boon and Bane of 60 GHz Networks: Practical Insights into Beamforming, Interference and Frame Level Operation [30]	COTS: Dell D5000 Docking station, Dell Latitude E7440 Laptop (2x8 antenna arrays) WiHD DVDO Air-3c (24 antenna arrays)	Vubiq 60 GHz receiver, Horn antenna (25 dBi), Agilent MSO-X 3034A Oscilloscope	Indoor	Frame length (ms), Normalized signal quality, PHY rate, TCP throughput (iperf)	Frame level, Beam pattern, Reflection (NLOS), Interference
4	Millimeter-Wave Blind Spots: Mitigating Deafness Collisions Using Frame Aggregation [32]	COTS: Dell D5000 Docking station, Dell Latitude 6430U Laptop	Vubiq 60 GHz receiver, Down-converter, Agilent MSO-X 3034A Oscilloscope	Indoor	Frame level, Throughput (Ostinato), Delay jitter (Wireshark)	Deafness effect
5	Steering with Eyes Closed: mm-Wave BeamSteering without In-Band Measurement [42]	Customized: Agilent E4432B signal generator, Vubiq 60 GHz transceiver (58-64 GHz, 1.8 GHz bandwidth and 16-QAM modulation) with omni-directional antenna, three horn antennas (beam width: 7°, 20° and 80°)	Tektronix TDS7054 Oscilloscope	Indoor 15x8 m room, TRx height of 1 - 1.5 m	Received signal strength (RSS)	Beamforming overhead

No	Work	DUT Hardware (60 GHz Transmitter)	Additional Receiver System	Environment	Measurement Parameters	60 GHz Issues
6	BeamSpy: Enabling Robust 60 GHz Links Under Blockage [26]	Customized: WiMi Transciever (57-64 GHz frequency band, 245.67 MHz bandwidth 10 dBm Tx power) Omni-directional antenna	Horn antenna (3° beamwidth)	Indoor	RSS (dB)	Link blockage, Beamforming overhead
7	Experimental Investigations of 60 GHz WLAN Systems in Office Environment [14]	Customized: 60 GHz Tx (2 dBm power) 800 MHz bandwidth, Horn antenna (18 dB and 20° HPBW), Mechanical rotator, Digital to Analog Converter (DAC), FPGA Board	60 GHz Rx, Horn antenna, Mechanical rotator, Analog to Digital Converter (ADC)	Indoor Room 3x4.5x3 m and cubicle	RSS (dB), Signal-to-Noise Ratio (SNR)	Reflection, Polarization
8	Demystifying 60 GHz Outdoor Picocells [35]	COTS: Dell D5000 Docking station, Dell 6430U Laptop (EIRP = 23 dBm) Customized: HXI Gigalink 6451, Horn antenna (25 dBi and 10° beamwidth) & Rotator	-	Outdoor	RSS, Throughput (iperf)	Distance, Reflection, Human blockage, User movement & Interference

No	Work	DUT Hardware (60 GHz Transmitter)	Additional Receiver System	Environment	Measurement Parameters	60 GHz Issues
9	Empirical Characterization of mm-wave Communication Links in Realistic Indoor Scenarios [31]	Customized: Agilent 81180A Signal generator Hittite Microwave HMC6000/1, and max. Tx power of 12 dBm OFDM: 4-QAM modulation SiversIMA FC1005V/00, max. Tx power of 16 dBm, horn antenna (10 dBi & 25 dBi), OFDM: BPSK, QPSK and QAM HXI GigaLink 6651, max. Tx power of 0.5 dBm horn antenna (10 dBi & 25 dBi), Single carrier: On-Off Keying	Agilent 81960A Vector Signal Analyzer and Agilent 90804A Oscilloscope	Indoor	Bit Error Rate (BER), Throughput	Effect of Sub-carrier modulation, & distance on throughput performance
10	Demo: Spectrum-Agile mm-Wave Packet Radio Implementation on USRPs [43]	Customized: Host PC, USRP-2953R (60, 70 and 80 GHz), up-converter horn antenna	Host PC, USRP-2953R, down-converter, horn antenna	Indoor	-	-

No	Work	DUT Hardware (60 GHz Transmitter)	Additional Receiver System	Environment	Measurement Parameters	60 GHz Issues
11	60 GHz Outdoor Urban Measurement Study of the Feasibility of Multi-Gbps mm-Wave Cellular Networks [36]	Customized: Agilent E4438C ESG Vector Signal Generator, SiversIMA FC1005V/100 mm-Wave up-converter, (EIRP = 30 dBm, fc = 61.5 GHz)	Horn antenna, Agilent 11970V mixer, Agilent N9030A Spectrum Analyzer	Outdoor	RSS	Beam-misalignment
12	60 GHz Indoor Networking through Flexible Beams: A Link-Level Profiling [8]	Customized: WiMi system: WARP board (FPGA), DAC, 60 GHz RF, Horn antenna	WiMi system: Horn antenna, 60 GHz RF Rx, ADC, WARP board (FPGA)	Indoor	RSS	User mobility, Link blockage
13	Learning from Experience: Efficient Decentralized Scheduling for 60GHz Mesh Networks [44]	COTS: Dell D5000 Docking station Dell 6430U Laptop	-	Indoor	PHY rate	Deafness effect

No	Work	DUT Hardware (60 GHz Transmitter)	Additional Receiver System	Environment	Measurement Parameters	60 GHz Issues
14	Augmenting Data Center Networks with Multi-Gigabit Wireless Links [33]	Customized: HXI (10 mW), 2 antennas: 60° & 15° beamwidth	-	Indoor Data center	RSS, SNR (dB), Throughput (iperf)	Range, Interference, Power Consumption
15	Cutting the Cord: a Robust Wireless Facilities Network for Data Centers [34]	COTS: Dell D5000 Docking station Dell 6430U Laptop Customized: HXI Gigalink 6451 Radio, Horn antenna (10° beamwidth)	-	Indoor Data center	PHY rate, Latency, Throughput (iperf)	Range, Interference (angular separation)
16	Proactive Traffic Control Based on Human Blockage Prediction Using RGBD Cameras for mm-wave Communications [45]	COTS: Dell D5000 Docking station Dell Latitude E5440 Laptop	-	Indoor	Throughput (iperf) Latency,	Human blockage
17	Proactive Base Station Selection Based on Human Blockage Prediction Using RGB-D Cameras for mmWave Communications [25]	COTS: Dell D5000 Docking station Dell Latitude E5440 Laptop	-	Outdoor	Throughput (iperf)	Human blockage, Relay using two active links simultaneously

No	Work	DUT Hardware (60 GHz Transmitter)	Additional Receiver System	Environment	Measurement Parameters	60 GHz Issues
18	Influence of Human Activity on Wideband Characteristics of 60 GHz Indoor Radio Channel [9]	Customized: 60 GHz channel sounder (500 MHz bandwidth)	-	Indoor 10 x 13 m	Attenuation (dB) Shadowing duration (ms)	Human blockage
19	Modeling Human Blockers in Millimeter Wave Radio Links [24]	Customized: R&S SMF100A signal generator (10 GHz sine wave), R&S SMZ90 multiplier V-band horn antenna (24 dBi)	V-band horn antenna (24 dBi), N12-3387 LNA, FS-Z90 mixer, FSQ26 VSA	Indoor 8 x 10 m	Attenuation (dB)	Human blockage
20	Characterization of 60 GHz Shadowing by Human Bodies and Simple Phantoms [23]	Customized: Agilent E8361A VNA, Power amplifier (20 dB), Horn antenna (20 dB) Vertical polarization (V-V)	Horn antenna (20 dB gain), LNA (30 dB), Agilent E8361A VNA	Indoor	Attenuation (dB) Reflection loss (dB)	Human blockage
21	Experimental Analysis of Human Body Effects on NLOS 60 GHz Propagation Channel [46]	Customized: Channel sounder (59.6-60 GHz)	-	Indoor (Corridor)	Normalized signal quality	Human blockage

Table B.1: Comparative review of 60 GHz experimental studies